A&A 475, 199–207 (2007)
DOI: 10.1051/0004-6361:20077624

Astronomy & Astrophysics

Host galaxy subtraction of TeV candidate BL Lacertae objects⋆

K. Nilsson[1], M. Pasanen[1], L. O. Takalo[1], E. Lindfors[1,2], A. Berdyugin[1], S. Ciprini[1,3], and J. Pforr[4]

[1] Tuorla Observatory, University of Turku, Väisäläntie 20, 21500 Piikkiö, Finland
e-mail: kani@utu.fi
[2] Metsähovi Radio Observatory, Helsinki University of Technology, 02540 Kylmälä, Finland
[3] INFN Perugia & Physics Dept., University of Perugia, via Pascoli, 06123 Perugia, Italy
[4] Landessternwarte Heidelberg, Königstuhl, 69117 Heidelberg, Germany

Received 10 April 2007 / Accepted 8 September 2007

ABSTRACT

Context. Photometric monitoring of active galactic nuclei is often complicated by the presence of a strong host galaxy component, which adds unwanted flux to the measurement and introduces a seeing-dependence to the flux that can plaque e.g. microvariability studies. We are currently monitoring a sample of 24 TeV candidate BL Lacertae objects, many of which exhibit a prominent host galaxy component, using differential aperture photometry.
Aims. In order to study our light curves free from the above effects, we have derived the host galaxy flux in differential aperture photometry as a function of aperture radius and *FWHM* for 20 resolved sources in our sample.
Methods. We created accurate surface brightness models of the targets and any significant nearby sources using high-resolution *R*-band imaging obtained at the Nordic Optical Telescope (NOT) and performed differential aperture photometry of the models over a grid of aperture radii and *FWHM* values.
Results. The results are given as correction tables, that list the fluxes (in mJy) of all "contaminating" sources (host galaxy + significant nearby objects) as a function of aperture radius and *FWHM*. We found that the derived fluxes depend strongly on aperture radius, but the *FWHM* has only a minor effect (a few percent). We also discuss the implications of our findings to optical monitoring programs and potential sources of error in our derived fluxes. During this work we have also constructed new calibration star sequences for 9 objects and present the finding charts and calibrated magnitudes.

Key words. galaxies: active – BL Lacertae objects: general – techniques: photometric – methods: data analysis

1. Introduction

BL Lacertae objects (BL Lacs) are a class of active galactic nuclei (AGN) characterized by weak or absent emission lines, variability of flux over the whole electromagnetic spectrum and high optical and radio polarization. Together with the flat spectrum radio quasars (FSRQs) they form the group of blazars (e.g. Urry & Padovani 1995). The spectral energy distribution of blazars has two broad peaks, one at the mm–UV region and another at the X-ray–gamma ray region (e.g. Fossati et al. 1998). The lower energy peak is very likely synchrotron radiation arising from relativistic electrons spiralling in a magnetic field. Various models have been proposed for the origin of the high energy peak. The most popular models involve inverse Compton (IC) scattering of soft photons from the same electrons that produce the synchrotron radiation (e.g. Maraschi et al. 1992; Bloom & Marscher 1996). These models predict correlations and time delays between the low- and high-energy emission, thus emphasizing the importance of long-term flux monitoring covering a wide range of frequencies.

In the optical-NIR region the monitoring efforts are sometimes hampered by the presence of a strong host galaxy component and/or nearby companions. Results obtained both from the ground (Falomo 1996; Heidt et al. 1999; Falomo & Kotilainen 1999; Pursimo et al. 2002; Nilsson et al. 2003) and using the HST (Urry et al. 1998; Urry et al. 2000; Falomo et al. 2000; Scarpa et al. 2000b) have shown the host galaxies of BL Lacertae objects to be bright ($M_R \sim -23.1$[1]), large ($r_e \sim 7$ kpc) and fairly round ($\epsilon = 0.1$–0.3) elliptical galaxies, whose bulk properties do not differ significantly from the population of inactive giant ellipticals. The luminosity evolution of the BL Lacertae host galaxies seems to be consistent with passive evolution from a fairly distant ($z = 2$–3) formation epoch (Heidt et al. 2004; O'Dowd & Urry 2005), but these results need to be confirmed with more complete samples.

Many BL Lacs also seem to have nearby companion galaxies at small (<50 kpc) projected distances (e.g. Falomo 1996; Falomo & Ulrich 2000), but in most cases there is no spectroscopic confirmation of real physical association between the BL Lac host and its companion. Like in the case of quasars, it has been speculated that tidal interaction between the BL Lac host galaxy and a companion galaxy might have triggered the nuclear activity (e.g. Heidt et al. 1999). In some objects clear signs of tidal interaction can be seen (e.g. 3C 371, Stickel et al. 1993), but this scenario needs be tested quantitatively with carefully selected samples and proper control samples. One argument against the interaction scenario is that BL Lac host galaxies appear very symmetric with no obvious signs of recent strong interaction.

The optical fluxes of BL Lacs are most commonly measured from CCD images in differential photometry mode, i.e. by

⋆ Appendices A and B are only available in electronic form at http://www.aanda.org

[1] Throughout the paper we use $H_0 = 70$ km s^{-1} Mpc^{-1}, $\Omega_m = 0.3$ and $\Omega_\Lambda = 0.7$.

comparing the BL Lac brightness to the brightness of several calibrated comparison stars in the field of the object. In this way changes in sky transparency can be eliminated and accuracies <1% attained even under varying conditions. The images are usually measured using aperture photometry, i.e. by integrating the light inside a circular aperture, whose radius is determined by the angular extent of the source and by the *FWHM*. Howell (1989) determined the optimal extraction aperture (i.e. the one that maximizes S/N) for point sources to be $r_{\rm opt} \sim FWHM$ and to depend slightly on the brightness of object on the CCD.

The presence of a strong host galaxy component can affect aperture photometry at least in two ways. Firstly, the host galaxy adds flux to the measurement aperture. Since the amount of the additional flux depends on the aperture radius, it is difficult to compare observations made using different apertures. In some cases the host galaxy contribution can exceed the nuclear flux by a large margin. In these cases the broadband spectra are highly distorted and relative flux variations underestimated in the optical region, unless a correction for the host galaxy contribution is determined.

Secondly, as discussed by Carini et al. (1991) and Cellone et al. (2000), *FWHM* changes during the observations may introduce false variability in objects with a prominent host galaxy component. This is due to the fact that stars and galaxies have different surface brightness profiles and thus they respond differently to changes in the *FWHM*. This effect is generally not very strong (0.01–0.03 mag; Cellone et al. 2000, and this work), but it may nevertheless affect studies that look for very low-level intranight variability. The seeing effect can be further amplified by nearby stars and galaxies, whose flux may leak into the measurement aperture in a seeing-dependent manner.

Since the nearby environments and the relative contribution of the host galaxy vary from one source to another, it is impossible to give a general formula for the aperture photometry correction. Instead, each case has to be studied separately. The goal of this study is to derive accurate aperture and seeing corrections for a sample of BL Lacertae objects that we are currently monitoring at Tuorla Observatory, taking also into account possible nearby stars and/or companion galaxies. We also want to derive some general conclusions with respect to optimizing aperture photometry for host galaxy contaminated objects. In Sect. 2 we will describe our sample and in Sect. 3 our analysis method in more detail. Section 4 gives the results of our analysis and Sect. 5 summarizes our findings.

2. The sample

We are currently running an *R*-band monitoring program at Tuorla Observatory of a sample of 24 BL Lacertae objects, comprising of all sources in Costamante & Ghisellini (2002) with $\delta > +20°$. These sources were selected as likely TeV emitters by Costamante & Ghisellini (2002), based mainly on their location in the radio – X-ray flux plane. With the advent of new large collection area Čerenkov telescopes (e.g. MAGIC; Lorenz 2004 and HESS; Hofmann et al. 2001) it is likely that these sources will be targets of extensive monitoring campaigns. Thus we started in fall 2002 to monitor these sources in the *R*-band with the aim of providing a long-term light curve to better constrain their variability characteristics and to alert the MAGIC-telescope of a possible high state of the sources (see Albert et al. 2006 for a successful trigger). Many of the sources in the list have been extensively monitored in the past decades (e.g. BL Lac, Mrk 501 and OJ 287), whereas for some of the sources only scattered points exist in the literature (e.g. 1ES 0033+595 and RGB J0136+391).

Table 1. An observing log of the new observations.

Object	Date	$t_{\rm exp}$ [s]	*FWHM* [arcsec]
1ES 1028+511	09 Feb. 2007	400	0.70
RGB J1117+202	08 Feb. 2007	600	0.72
1ES 1426+428	08 Dec. 2007	720	0.64
1ES 1544+820	27 Sep. 2005	720	1.8
OT 546	27 Sep. 2005	720	2.1

The monitoring is made by obtaining CCD-images of the sources using Tuorla 1.03 m and KVA 0.35 m telescopes and measuring the source and suitable comparison stars with aperture photometry. The aperture radius is fixed for each source to 4.0–7.5 arcsec depending on the brightness of the source. The flux of the source is obtained via normal differential photometry using one of the comparison stars as a primary reference and the rest as a check of the stability of the comparison star and general quality of the photometry. Calibrated *R*-band magnitudes are obtained by using published comparison star magnitudes or comparison sequences calibrated by ourselves (see Appendix A). The magnitudes are also corrected for the color difference between the object and the comparison star using the calibrated color coefficients of the telescopes.

3. Analysis

Of the various factors affecting aperture photometry of host galaxy dominated sources, we will concentrate on the two most important factors: the aperture radius and *FWHM*. There are other factors that may contribute noise, such as aperture centering and sky determination errors, but in the following we will assume that these factors are controlled by e.g. using an appropriate symmetry clean algorithm in the aperture centering and careful selection of the sky region.

There are at least two methods one can use to estimate the host galaxy contribution. Firstly, one can fit two-dimensional models consisting of an unresolved nuclear component and a host galaxy component to each monitoring frame and use the fitted nuclear magnitude as the result. This is rarely feasible, however, owing to too poor resolution and too low signal to noise in typical monitoring frames, which makes it impossible to properly characterize the host galaxy. In addition, the noise inherent to the fitting process can increase the total noise into unacceptable levels, especially for sources with strong host galaxy components. Furthermore, nearby stars and galaxies may be difficult to mask out from the fit. The advantage of this method is that if the PSF is determined from the observed frame, the effect of the PSF shape is canceled, unless it varies considerably over the field of view.

In the second method one fits two-dimensional models to high-resolution, high-S/N images of the sources and computes aperture correction tables through simulated frames. This method, in addition to being computationally more effective, has the advantage that the fitting process is far more accurate than in the case of fitting single monitoring frames. Further advantage of this approach is that through simulated frames one can gain insight on the relative importance of the factors (aperture size, PSF shape) under investigation. There is one drawback of this method with respect to the first one: in real monitoring data there is a high variation of PSF shapes due to e.g. optical imperfections and tracking errors. Since it is impossible in practice to compute correction tables for every possible PSF shape, one has to focus

Table 2. The photometric parameters adopted for the host galaxies and nearby companions of the objects in this study. Column 3 gives the *FWHM* of the observation and Cols. 5 and 6 give the offset (in arcsec) relative to the BL Lacertae nucleus. Values listed in parentheses were held constant during the fitting (see Sect. 3 for details of the modeling).

Object	z	*FWHM* (arcsec)	Type	Δx (arcsec)	Δy (arcsec)	R mag	$r_{\rm eff}$ (arcsec)	ell	PA (deg)	β	Ref.
1ES 0033+595		1.13	star	1.4	–0.7	17.88 ± 0.03					1, 4[1]
1ES 0120+340	0.272	1.04	host	0.0	0.0	17.89 ± 0.07	2.0 ± 0.2	0.08 ± 0.02	137 ± 46	0.12 ± 0.02	4
			star	–0.4	6.4	17.11 ± 0.04					1
RGB J0214+517	0.049	0.76	host	0.0	0.0	14.08 ± 0.07	17.4 ± 1.1	0.15 ± 0.01	132±1	0.12 ± 0.01	4
			star	–6.1	0.3	17.14 ± 0.06					1
1ES 0806+524	0.138	0.99	host	0.0	0.0	16.10 ± 0.07	4.6 ± 0.2	0.10 ± 0.02	106 ± 4	0.14 ± 0.02	1
1ES 1011+496	0.212	0.96	host	0.0	0.0	16.41 ± 0.09	4.0 ± 0.6	0.28 ± 0.03	42 ± 4	0.06 ± 0.01	4
1ES 1028+511	0.360	0.70	host	0.0	0.0	18.60 ± 0.22	2.0 ± 4.7	0.34 ± 0.19	152 ± 44	(0.25)	1
Mrk 421	0.031	0.53	host	0.0	0.0	13.18 ± 0.05	8.2 ± 0.2	0.21 ± 0.01	105 ± 1	0.36 ± 0.02	3
			galaxy[2]	–11.4	8.3	15.54 ± 0.04	7.3 ± 0.1	0.39 ± 0.01	81 ± 1	(0.25)	1
			galaxy[2]	–11.4	8.3	16.51 ± 0.04	3.0 ± 0.1	0.79 ± 0.01	66 ± 1	(1.00)	1
RGB J1117+202	0.139	0.72	host	0.0	0.0	16.31 ± 0.13	4.6 ± 0.6	0.22 ± 0.03	162 ± 5	0.28 ± 0.07	1
			galaxy	–8.1	–3.7	18.23 ± 0.05	0.9 ± 0.1	0.11 ± 0.03	94 ± 8	(0.25)	1
			galaxy	10.8	4.1	17.79 ± 0.06	2.3 ± 0.1	0.33 ± 0.02	75 ± 2	0.38 ± 0.02	1
			star	4.8	10.0	19.99 ± 0.05					1
Mrk 180	0.045	1.17	host	0.0	0.0	14.08 ± 0.05	8.3 ± 0.3	0.05 ± 0.01	15 ± 3	0.19 ± 0.01	4
			star	–0.6	–6.3	15.21 ± 0.04					1
RGB J1136+676	0.135	0.96	host	0.0	0.0	15.93 ± 0.05	4.1 ± 0.2	0.13 ± 0.01	130 ± 3	0.16 ± 0.01	4
			galaxy	6.4	6.0	19.14 ± 0.32	0.6 ± 0.3	0.09 ± 0.08	162 ± 54	0.13 ± 0.21	1
ON 325	0.130	1.10	host	0.0	0.0	15.26 ± 0.32	19.4 ± 6.2	0.11 ± 0.05	13 ± 22	0.04 ± 0.06	4
			galaxy	2.1	–2.5	18.90 ± 0.05	0.5 ± 0.1	0.40 ± 0.03	89 ± 2	(0.25)	1
1ES 1218+304	0.182	1.61	host	0.0	0.0	16.86 ± 0.03	3.6 ± 0.3	0.24 ± 0.02	88 ± 2	(0.25)	1
			star	–15.1	1.3	15.59 ± 0.03					1
RGB J1417+257	0.237	0.54	host	0.0	0.0	16.66 ± 0.06	5.2 ± 0.3	0.14 ± 0.02	166 ± 3	(0.25)	1
			galaxy	1.8	–4.8	18.14 ± 0.23	2.6 ± 0.7	0.34 ± 0.05	139 ± 5	0.22 ± 0.11	1
1ES 1426+428	0.129	0.64	host	0.0	0.0	15.93 ± 0.05	4.2 ± 0.2	0.37 ± 0.01	118 ± 1	0.21 ± 0.02	1
1ES 1544+820		1.83	star	–0.1	–4.1	17.88 ± 0.03					1
Mrk 501	0.034	0.72	host	0.0	0.0	11.92 ± 0.06	48.2 ± 4.2	0.24 ± 0.01	169 ± 1	0.09 ± 0.01	3
OT 546	0.055	2.08	host	0.0	0.0	15.48 ± 0.08	4.9 ± 0.4	0.14 ± 0.03	40 ± 7	0.24 ± 0.03	1
1ES 1959+650	0.047	0.67	host	0.0	0.0	15.08 ± 0.03	6.4 ± 0.1	0.21 ± 0.01	97 ± 1	0.44 ± 0.02	1,2
			star	6.5	8.2	16.94 ± 0.03					1
BL Lac	0.069	0.77	host	0.0	0.0	15.05 ± 0.08	10.4 ± 0.9	0.43 ± 0.01	44 ± 1	0.19 ± 0.02	4
1ES 2344+514	0.044	0.63	host	0.0	0.0	13.90 ± 0.06	10.9 ± 0.6	0.25 ± 0.01	104 ± 1	0.19 ± 0.01	3
			star	9.0	10.3	15.24 ± 0.05					1

[1] References: (1) this work, (2) Heidt et al. (1999), (3) Nilsson et al. (1999), (4) Nilsson et al. (2003).
[2] The bulge and disk component of the companion galaxy.

on the most important features of the PSF. This somewhat limits the accuracy of the second method, but given its advantages, we have opted to use this method instead the first one. Furthermore, as we will show below, this method can produce corrections that are sufficiently accurate in most practical situations.

Our method of estimating host galaxy contribution thus consists of four steps: 1) obtain a deep high-resolution image of the object and fit a two-dimensional nucleus + host galaxy model to it, 2) create a simulated image of the object field with a proper comparison star sequence, nearby sources and the object *without* the nuclear component, 3) select the PSF shape and *FWHM* and and convolve the image with the selected PSF, 4) Perform aperture photometry of the simulated image. Steps 3 and 4 are repeated over a range of apertures and seeing conditions to build a correction table. Each of these steps is described in more detail below.

3.1. Observations

We have collected high-resolution R-band images of all 24 sources in our monitoring sample using the Nordic Optical Telescope (NOT) in 1995–2007. These images form a very homogeneous set of images with respect to instrumentation, resolution and S/N and they are thus ideal for our purpose. For 16 objects the photometric parameters of the host galaxies have been published elsewhere by us (see the references in Table 2). Renato Falomo kindly provided us with images of 3 objects (1ES 0806+524, 1ES 1218+304 and RGB J1417+257) published in Falomo & Kotilainen (1999) and we have obtained new images of 5 objects using the ALFOSC instrument at the NOT (see Table 1).

3.2. Host galaxy decomposition

For maximum accuracy it is important to analyze all images in a homogeneous manner. The 16 previously published images were analyzed by us using homogeneous procedures and thus satisfy this requirement, but the 8 new objects need to be reanalyzed before proceeding to the next phase. Below we will give a short description of our host galaxy analysis (see Nilsson et al. 1999, for details).

The two-dimensional model of the source is assumed to consist of two components, an unresolved nucleus parametrized by its position ($x_{\rm c}$, $y_{\rm c}$) and magnitude $m_{\rm c}$ and the host galaxy parametrized by position ($x_{\rm g}$, $y_{\rm g}$), total magnitude $m_{\rm g}$, major axis effective (half-light) radius $r_{\rm e}$, ellipticity ϵ, position angle PA and slope of the brightness profile β. The host galaxy surface brightness $I(r)$ is assumed to follow the Sérsic law

$$I(r) = I(r_{\rm e}){\rm dex}\left\{-b_\beta\left[\left(\frac{r}{r_{\rm e}}\right)^\beta - 1\right]\right\}, \quad (1)$$

where b_β is a β-dependent constant. The model is convolved with a PSF obtained from sufficiently bright stars in the field. Prior to fitting any overlapping stars/galaxies are masked out from the fit. The 10 free parameters (3 for the core and 7 for the galaxy) are then fitted to the observed image by minimizing the chi squared between the observed image and the model using an iterative Levenberg-Marquardt loop.

The same fitting procedure is also applied to any significant nearby stars and/or galaxies, except that the stars consist of only the nuclear component and the galaxies of only the galaxy component. To be considered significant a galaxy or a star must be closer than 20″ to the source and brighter than $m_g + 4.0$.

The results of the fitting procedure are given in Table 2. We also show the surface brightness decomposition of the newly observed sources in Fig. 1. As already noted in Nilsson et al. (2003), the host galaxies are large ($r_e \sim 7$ kpc) and luminous ($M_R \sim -23$) elliptical galaxies, whose surface brightness closely follows the Sérsic law.

Altogether 4 sources (1ES 0033+595, RGB J0136+391, 1ES 0647+250 and 1ES 1544+820) were found to be completely unresolved with no signs of the host galaxy, 2 (3C 66A and OJ 287) marginally resolved and 18 clearly resolved. In the two marginally resolved objects a faint host galaxy component can be detected, but the significance of this detection does not exceed the formal limit set in Nilsson et al. (2003), namely that $r_e > 5\sigma_{r_e}$, where σ_{r_e} is determined from simulations. The host galaxy in these two objects can have a small effect on aperture photometry, but given the uncertainties in their host galaxy parameters we have left them out in the following. Note, however, that two of the unresolved sources (1ES 0033+595 and 1ES 1544+820) have significant nearby stars that need to be taken into account. Our final list in Table 2 thus incorporates 20 objects of the monitoring sample with a significant host galaxy component and/or nearby companions. Note that the host galaxy magnitudes in Table 2 slightly differ from already published values due to the different calibration adopted in this study, explained in more detail below.

3.3. Photometric calibration

For maximum accuracy, the the host galaxy fits should be calibrated in exactly the same way as the differential photometry. Since the latter is calibrated using comparison stars in the object field, ideally the deep host galaxy images should contain the same comparison stars. However, this was the case for three objects only (ON 325, OT 546 and 1ES 1959+650), in the rest the comparison stars were either out of the field of view or strongly saturated. For these sources we first selected 1–3 relatively bright (but unsaturated) stars from the deep images and determined their R-band magnitudes using our ∼4 years of monitoring data with the comparison stars in Table 3 as calibrators. This effectively ties the deep images to the same scale with our photometry, although the uncertainty of the host galaxy increases due to the adoption of secondary (and more noisy) calibrators.

3.4. Modeling and aperture photometry

After the model fitting and photometric calibration we created simulated master fields of all objects in Table 2 (see Fig. 2). These fields contained the host galaxy (without the BL Lac nucleus), any nearby sources and the primary comparison star(s) in Table 3. The models were made with the same pixel scale and software as in the model fitting, thus ensuring accurate representation of the light distribution in the original images. After this, the master fields were convolved with three different PSF profiles (Moffat profiles with $\beta = 2.0$, 2.5 and 3.0) over a grid of *FWHM* values 0.5, 1.0 ..., 8.0 arcsec, resulting in 48 modeled fields per object.

The simulated fields were then measured with aperture photometry using the same procedure and software as for the real monitoring data, i.e. the primary comparison stars were used as calibrators and the magnitudes were corrected for the color difference between the object and the comparison stars using calibrated color coefficients. We generally do not know the $(V - R)$ color of the host galaxies, thus we assumed $(V - R) = 0.6$ for them, corresponding to an early-type galaxy at $z = 0$. As the host galaxies of all our sources are early type galaxies at relatively low redshifts, and the $(V - R)$ color coefficients relatively small (<0.1), this assumption does not introduce large errors. For the measurements we used aperture radii of 0.5, 1.0, ..., 10.0 arcsec, covering the expected range of aperture radii in long-term photometric monitoring programs.

Table 3. Adopted primary comparison star magnitudes.

Object	Star	R	$(V - R)$	Ref.[1]
1ES 0033+595	D	13.66 ± 0.03	1.46	1
1ES 0120+340	C	13.12 ± 0.03	0.38	1
RGB J0214+517	A	13.85 ± 0.05	0.51	1
1ES 0806+524	C2	14.22 ± 0.04	0.39	3
1ES 1011+496	E	14.04 ± 0.03	0.39	1
1ES 1028+511	1	12.93 ± 0.03	0.27	5
Mrk 421	1	14.04 ± 0.02	0.32	5
RGB J1117+202	E	13.56 ± 0.04	0.42	1
Mrk 180	1	13.73 ± 0.02	0.25	5
RGB J1136+676	D	14.58 ± 0.04	0.46	1
ON 325	B	14.59 ± 0.04	0.37	2
1ES 1218+304	B	13.61 ± 0.01	0.40	4
RGB J1417+257	A	13.78 ± 0.04	0.57	3
1ES 1426+428	B	14.17 ± 0.02	0.44	4
1ES 1544+820	D	12.87 ± 0.03	0.31	1
Mrk 501	4	14.96 ± 0.02	0.34	5
	5	15.08 ± 0.02	0.43	5
	6	14.99 ± 0.04	0.68	5
OT 546	B	12.81 ± 0.06	0.33	2
1ES 1959+650	4	14.08 ± 0.03	0.45	5
	6	14.78 ± 0.03	0.42	5
BL Lac	C	13.79 ± 0.05	0.47	2
1ES 2344+514	C1	12.25 ± 0.04	0.36	3

[1] References: (1) this work, (2) Fiorucci & Tosti (1996), (3) Fiorucci et al. (1998), (4) Smith et al. (1991), (5) Villata et al. (1998).

4. Results and discussion

The R-band host galaxy fluxes resulting from the above procedure are given in the Tables B.2–B.21 in Appendix B (available online only, see Table B.1 for an example). The fluxes are given as a function of aperture radius and *FWHM* (in arcsec) for the $\beta = 2.5$ convolution kernel. Note that we show the data only for aperture radii and *FWHM* larger than the resolution of the deep R-band images. In Fig. 3 we show an example of the host galaxy magnitude as a function of *FWHM* and three aperture radii. The figure illustrates well the most important aspects of the data,which we discuss now in more detail.

As can be expected, the host galaxy brightness depends strongly on the chosen aperture radius. The dependence on *FWHM* is smaller, typically a few hundreds of a magnitude even

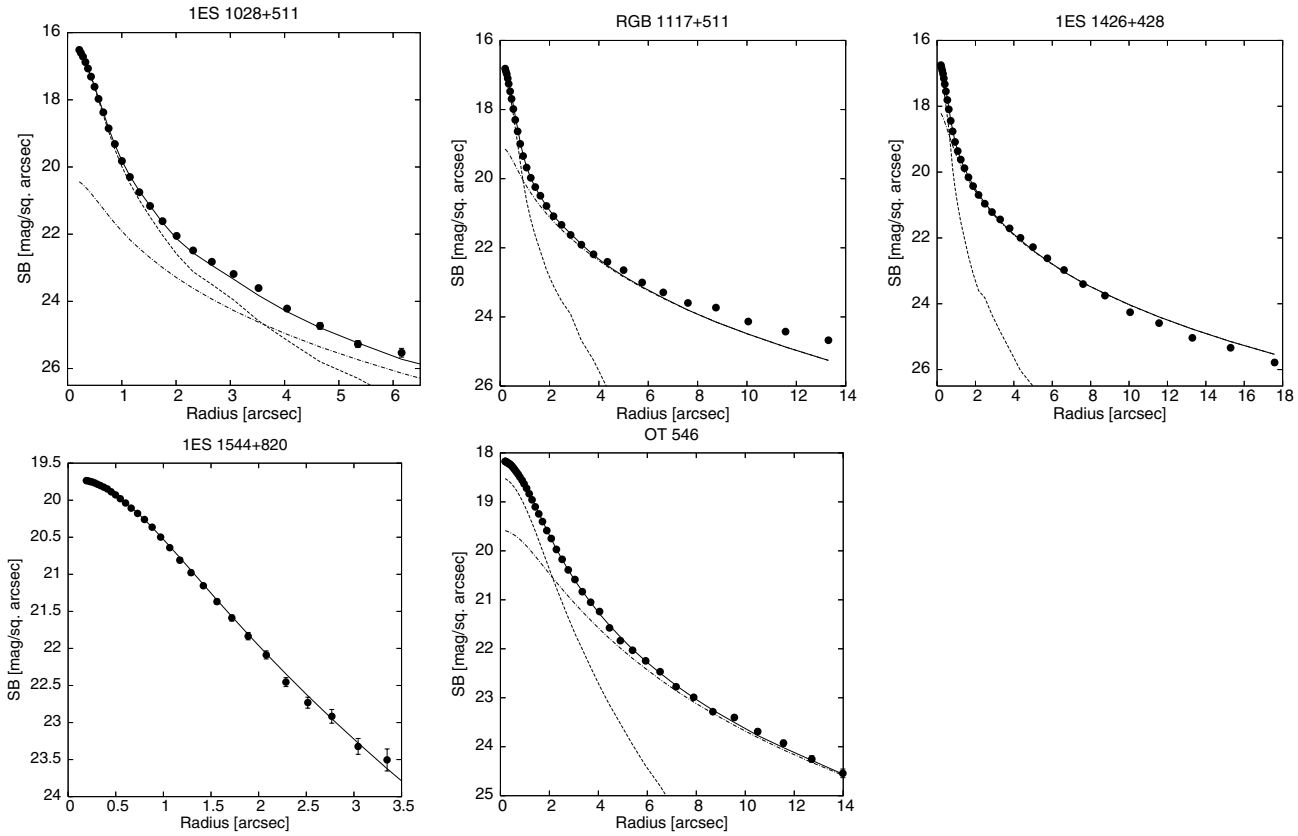

Fig. 1. Surface brightness profiles of the newly observed sources. The circles denote the observed surface brightness and the solid line the modeled (core+host galaxy) surface brightness. The core and host galaxy surface brightness are indicated by dashed and dot-dashed lines, respectively. Note that 1ES 1544+820 is unresolved and only a core-model is shown.

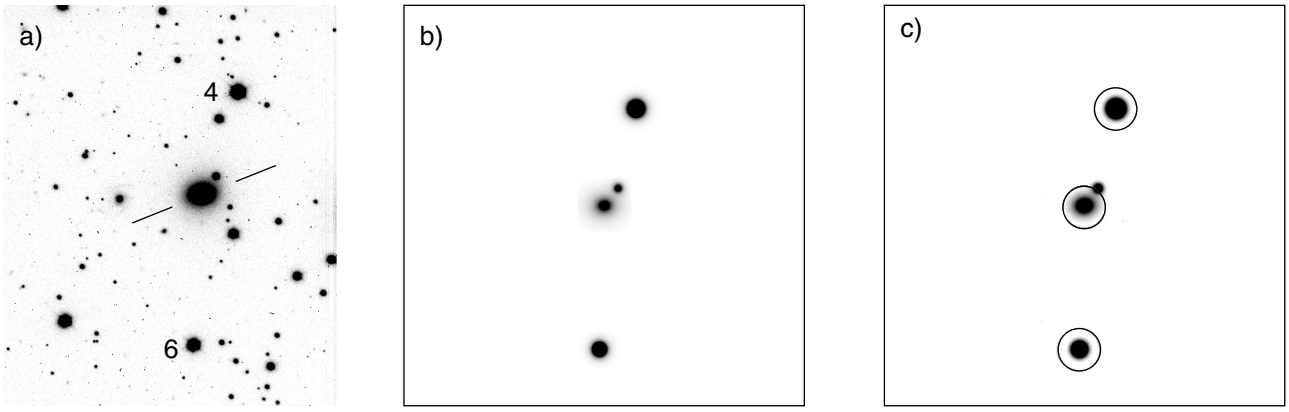

Fig. 2. An example of the modeling procedure: **a)** An *R*-band image of 1ES 1959+650 obtained with the NOT with a *FWHM* of 0.″7. The field size is 2.5 × 3.0 arcmin. The primary comparison stars 4 and 6 from Villata et al. (1998) have also been marked. **b)** The simulated field, convolved to a *FWHM* of 3.″0 with a $\beta = 2.5$ Moffat profile. **c)** The aperture photometry with an aperture radius of 10.″0. Note that using a large aperture includes a substantial fraction of the nearby star.

for large (factor of two) changes of *FWHM*. Note that the curves in Fig. 3 are valid for the host galaxy only. Normally there is a nuclear component present, which makes the dependence on seeing even smaller. Thus the dependence on seeing is probably too small to be of importance, with the exception of microvariability studies where very small amplitude variations are looked for (Cellone et al. 2000).

We next study the possibility to reduce all observations to the same aperture radius and *FWHM* using our 4 years of monitoring data as a test bench. We measured the light curves of the objects in Table 2 using three different aperture radii, 5.0, 7.5 and 10.0 arcsec. The median *FWHM* of our observations is 3.4 arcsec, so the smallest aperture probably best matches our typical seeing and the largest would rarely be used in real monitoring work. We nevertheless consider all three here for an illustrative example. The *FWHM* was determined by fitting $\beta = 2.5$ Moffat profiles to the stellar images in each monitoring frame. The host galaxy magnitude corresponding to the aperture radius and *FWHM* was then looked from Tables B.2–B.21, the host-subtracted magnitude computed for each frame, and all fluxes within one night (typically 3–4) were averaged.

In Fig. 4 we show one example of the outcome of this procedure. The left panel shows the light curves of Mrk 501 using the three aperture radii. The presence of the host galaxy is clearly

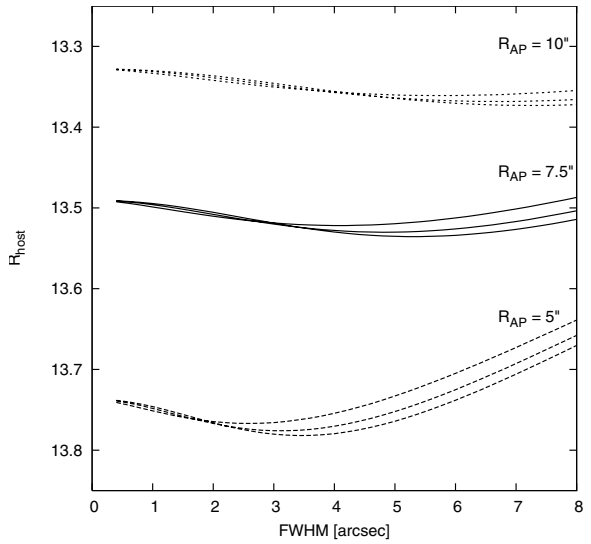

Fig. 3. The host galaxy magnitude of Mrk 501 as a function of *FWHM* and three aperture radii. The three curves for each aperture correspond to the three different convolution kernels (Moffat β = 2.0, 2.5 and 3.0).

revealed by the increasing average object brightness with increasing aperture radius. This should not happen with point sources since we are using *differential* aperture photometry, unless there are e.g. large PSF variations across the field of view. The shape of the light curve is independent of aperture radius, except that the light curves measured with larger aperture are noisier due to too large aperture with respect to the seeing.

The right panel shows the same light curves after reducing all measurements to a 7.″5 aperture radius. The average levels of the light curves agree now much better, the difference between average levels of 7.″5 and 5″ curves is now 0.9%, compared to 13.8% before the correction. The corresponding values between the 7.″5 and 10″ curves are 1.0% and 11.0% Similar improvement is observed in all 20 light curves. This is summarized in Fig. 5, where we show the differences between 7.″5 and 5″ and 7.″5 and 10″ light curves before and after the corrections (in percent). The distributions after the correction are concentrated around zero with an average of (0.0±0.4) for the lower left distribution and (–0.1 ± 0.3) for the lower right distribution, showing that on average the correction works very well. The standard deviations of the distributions are 1.5 and 1.2 for the lower left and lower right distributions, respectively. These numbers represent the accuracy one can expect for these sources when trying to reduce observations made with different aperture radii into the same aperture. For instance, if observations are measured with 5.0 and 7.5 arcsec radii, one can expect the measurements to agree within 1–2% (depending on the source) after the correction.

We have also looked at similar distributions as in Fig. 5 for pure nuclear fluxes, i.e. after subtraction of the host galaxy correction. In this case the relative accuracy is lower, simply due to the fact that pure nuclear fluxes are lower than total fluxes. The distributions of the corrected fluxes have now standard deviations of 4.7% (7.5 vs. 5.0 arcsec aperture) and 4.0% (7.5 vs. 10.0 arcsec aperture). The total range is –7.3% to 13.8% (7.5 vs. 5.0 arcsec) and –6.5% to 12.1% (7.5 vs. 10.0 arcsec), showing that differences over 10% in nuclear fluxes are possible after correction for the host galaxy.

The above results emphasize the importance of using the same aperture radius between different observers in large monitoring campaigns. In principle the tables in Appendix B could be used to reduce all data into the same aperture, but in practice the accuracy of this correction may not be sufficient for all applications. In large monitoring campaigns it is thus far better to secure in advance that all parties are using the same aperture when performing reductions than try to correct for different aperture sizes afterwards.

We finally mention an example of the application of the tables in Appendix B. Our optical monitoring work is mainly done to support the TeV observations by the MAGIC-telescope on La Palma. In this work it is important to subtract the host galaxy contribution correctly to build an accurate SED and to correctly estimate the relative variability amplitude. Host galaxy subtraction thus forms an important step before using the data for comparisons with the models. As already mentioned, the host galaxy flux can be a substantial fraction of the total flux. For instance, the average optical flux of 1ES 2344+514 during the four years of our monitoring is 4.43 mJy (using an aperture radius of 7.5 arcsec) with an rms scatter of 0.1 mJy, i.e. 2.2% of the average level. However, from Table B.21 we see, that the host galaxy flux at 7.5 arcsec aperture radius and 3 arcsec *FWHM* (closest to our average *FWHM* of 3.4 arcsec) is 3.71 mJy, i.e. the true nuclear flux is only 0.72 mJy and the 0.1 mJy rms variability corresponds to 14% of the mean level. The above example shows how important it is to properly subtract the host galaxy contribution before proceeding with the analysis.

4.1. Error analysis

The accuracy of our method depends mainly on three factors: 1) how accurately is the fitting procedure able to separate the nuclear component from the host galaxy component, 2) how accurately does the Sérsic model represent the true surface brightness profile and 3) how accurately can the deep *R*-band images be calibrated.

As noted by several authors before (e.g. Nilsson et al. 2003; Pursimo et al. 2002; Scarpa et al. 2000a) the differences between the host galaxy parameters derived by different authors tend to be significantly higher than the quoted error bars (see e.g. Fig. 3 by Nilsson et al. 2003, but note also that one should check that the same model and same definitions for the parameters are used when making the comparisons). For instance, the rms difference in the host galaxy magnitude is typically 0.2–0.3 mag, but the quoted error bars are typically a factor of 2–5 lower. The effective radius is notoriously difficult to constrain, with often factor of two differences for even well-resolved objects. These differences point to systematical errors that probably stem from many factors, such as the nucleus to host galaxy flux ratio (bright nuclei make it more difficult to constrain the host galaxy), redshift (distant host galaxies are fainter and smaller) the method of analysis, resolution, and signal to noise. For instance, by analyzing very high signal to noise NOT images Pursimo et al. (2002) found that the derived effective radius depends on the outer radius of the fit region with larger fit radii producing larger effective radii. Furthermore, they noted that for the apparently largest galaxies their values for effective radius were systematically larger than those obtained from HST data, which was attributed to relatively short exposures of the HST images.

Test simulations in Nilsson et al. (2003) showed that the host galaxy and nuclear parameters can be recovered without bias if the PSF has sufficiently high S/N and the apparent size of the host galaxy is sufficiently large (i.e. several times larger than the *FWHM*). Since these two conditions are fulfilled here (all our host galaxies are nearby, $z < 0.4$), the procedure is expected

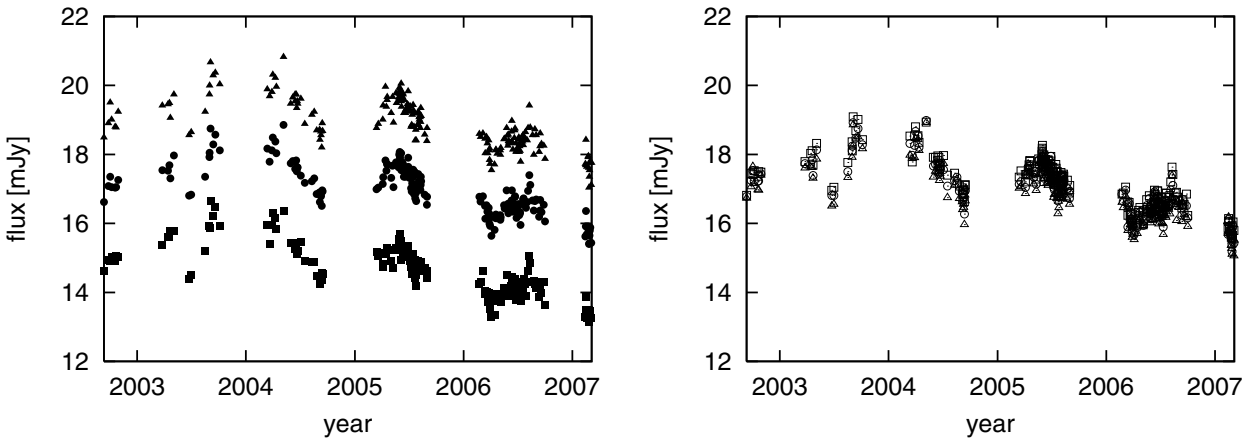

Fig. 4. The light curves of Mrk 501 before (*left*) and after (*right*) reducing all measurements to 7.″5 aperture radius using the host galaxy correction derived in this study. The curves on the left correspond to (*from top to bottom*) 10.0, 7.5 and 5.0 arcsec aperture radii. The same symbols have been used in both panels, except that in the right panel they are unfilled.

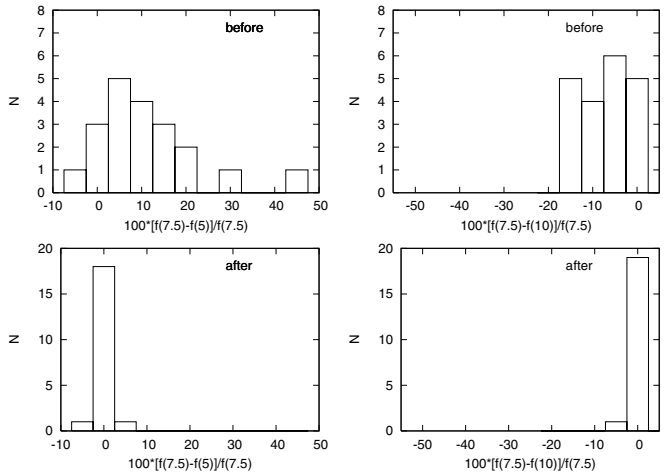

Fig. 5. The percent difference between 7.″5 and 5″ (*left*) and 7.″5 and 10″ (*right*) light curves before (*upper row*) and after (*lower row*) applying the host galaxy correction for all 20 sources.

to accurately separate the nuclear component from the host galaxy component and provide accurate morphological parameters (magnitude, effective radius, ellipticity and position angle) for the host galaxy. However, even with well-resolved images one may encounter problems in characterizing the host galaxy. Many elliptical galaxies exhibit deviations from a smooth Sérsic profile: disk components in their central parts (Scorza & Bender 1995), central "cusps" (Trujillo et al. 2004) and even dust lanes (e.g. 1ES 1959+650; Heidt et al. 1999). If the host galaxy surface brightness does not follow the Sérsic law, errors may in induced to the host galaxy magnitudes.

Considering the points above we have divided the total error into three components: the random error $\sigma_{\rm ran}$, the systematic error $\sigma_{\rm sys}$ and the calibration error $\sigma_{\rm cal}$. The random error arises from random noise in the images (photon and readout noise), from the errors in the assumed PSF shape and background determination errors. In a perfect situation, free of systematic effects, this would be the only source of noise. We created 30–50 simulated images for each source with the same noise characteristics as in the real data, an error in the background level and a realistic representation of PSF variations over the field of view (see Nilsson et al. 2003, for details). We then fitted a two-dimensional model to each image using the same procedures as with the real data. After this, the host galaxy flux was determined over the same grid of *FWHM* values and aperture radii as with the real data. Finally, the random error, $\sigma_{\rm ran}$, was computed as the standard deviation of the measured fluxes at each aperture radius and *FWHM*. Typically these errors are small (a few percent), except for very small aperture radii and small *FWHM* values and depending on the apparent size of the host galaxy.

As discussed above, systematic effects and deviations from a smooth Sérsic law are possible and thus should be included in the error estimate. Note however, that the errors in host galaxy magnitude and effective radius are correlated, i.e. any deviation in one parameter is "corrected" by the fitting procedure by adjusting the other to match the observed 2-d light distribution. Since we are mainly interested in the accuracy of the 2-d representation of the source and not the parameters themselves, the best way to estimate the systematic errors is to examine the model residuals. Any deviations from a Sérsic law or any systematic effects should be visible as nonzero residuals and can be quantified by measuring the residual fluxes over the aperture radii concerned here. The only type of error we cannot estimate properly is wrong separation of the host galaxy flux from the nuclear flux. For instance, if the host galaxy has a flattened profile at distances from the center smaller than our resolution, our model will overestimate the host galaxy flux and underestimate the nuclear flux. Due to insufficient resolution this may not be detected in the residual image.

Many objects in our sample show deviations from a smooth Sérsic profile e.g. due to interaction with a nearby companion galaxy or dust lanes. These deviations are usually not very large (from a few percent up to 20%) and they tend to be in the form of fluctuations around zero mean and thus mostly cancel out, especially when large aperture radii are used. Some sources (like RGB J1117+202; see Fig. 1) show larger deviations (up to 50%) in their outer parts. Since this happens at large distances from the object center and at low surface brightnesses, it has a very small effect in aperture magnitudes.

Hence, the systematic effects ($\sigma_{\rm sys}$) were estimated in the following way: the residual images (observed - model) were first convolved with $\beta = 2.5$ Moffat profiles to *FWHM* values 1.″0, 2.″0,..., 8.″0 and these images were measured with aperture radii 1.″0, 1.″5,..., 10.″0. The norm of the measured flux at each *FWHM* and aperture radius was then formally adopted as the systematic

error $\sigma_{\rm sys}$, giving us a very conservative estimate of the systematic error.

After computing $\sigma_{\rm ran}$ and $\sigma_{\rm sys}$ we compute the final error σ at each aperture radius and *FWHM* from

$$\sigma = \sqrt{\sigma_{\rm ran}^2 + \sigma_{\rm sys}^2 + \sigma_{\rm cal}^2}\,,$$

where $\sigma_{\rm cal}$ is the estimated error of the calibration (0.01–0.05 mag). Note that contrary to the tables in Appendix B the error bars in Table 2 contain the contributions from $\sigma_{\rm ran}$ and $\sigma_{\rm cal}$ only.

As a general remark we note that the relative error tends to be largest at small aperture radii and small *FWHM* values. This is understandable since the central regions are most sensitive to errors in the model parameters (large $\sigma_{\rm ran}$) and in the central parts deviations from a Sérsic profile and PSF error are also largest (large $\sigma_{\rm sys}$).

4.2. Future work

In the future this method can be easily extended to more objects and other wavelength bands. The only requirement is a high-resolution, high signal to noise image of the object at the given band. An important step would be a more detailed study of the influence of the PSF shape, presently assumed to be a Moffat $\beta = 2.5$ profile. In principle, the PSF could be determined from the image using a sufficiently bright star, the photometric model convolved with this PSF and the aperture correction computed for each frame individually, yielding a more accurate correction. This could potentially improve times series of objects with bright host galaxies. However, poor sampling and the fact that such stars are not always available could mean that this method is not always usable.

The method could also be used in imaging polarimetry, where dilution by the unpolarized host galaxy light makes it very difficult to estimate the true polarization of the BL Lac nucleus. Since many polarization techniques use aperture photometry, a similar technique than employed here could be used to overcome the dilution. Finally, the accuracy of the method at small aperture radii and small *FWHM* could be improved using HST images, since these allow a better characterization of the central parts of the host galaxies.

4.3. Notes on individual objects

1ES 0033+595: There is a star 1.6 arcsec away from this object with a comparable magnitude ($R = 17.9$) to the object ($R \sim 17.1$). This pair is unresolved in typical monitoring observations, and in practice one cannot center the aperture on 1ES 0033+595, unless the seeing is very good (<1 arcsec). In our simulations we have thus fixed the aperture center midway between 1ES 0033+595 and the star to make a more realistic simulation.

Mrk 421: Only one very faint star ($R = 17.5$) is available in the field as a PSF star and a secondary calibrator. Thus the errors for Mrk 421 are larger than for the other well-resolved objects.

RGB J1117+202: Our model underestimates the host galaxy brightness at large radii. It is possible that the galaxy is interacting with the two nearby galaxies thus distorting its shape, although no clear signs of interaction are visible. This affects very large apertures ($\gtrsim$8 arcsec) only.

1ES 1959+650: There is a weak dust lane in this galaxy roughly 1 arcsec North of the nucleus oriented in E-W direction (Heidt et al. 1999). This dust lane is not included in our model, but its effect is very small (<0.01 mag) judging from the photometry on the residual image.

BL Lac: The light from a bright ($R = 11.93$) star 24 arcsec E of this object enters the aperture at large seeing values and large apertures. Since this effect depends strongly on the PSF shape at the outer parts, we have not included it in our model, but taken it into account in our error estimates.

5. Conclusions

Photometric monitoring of active galactic nuclei is often complicated by the presence of a strong host galaxy component. The host galaxy distorts the optical fluxes and thus makes it difficult to estimate the SED and true variability level of the active nucleus. In addition, *FWHM* changes can induce false variability, which complicates e.g. microvariability studies.

In order to quantify these effects, we have measured the host galaxy flux for 20 BL Lacertae objects over a grid of aperture radii and *FWHM* values using high-resolution images obtained at the Nordic Optical Telescope (NOT). In addition to the host galaxy, we have also included the flux from any nearby stars or galaxies that could contribute significantly inside the measurement aperture. Two-dimensional model fitting was employed to separate the nuclear component from the host galaxy component and to determine the photometric parameters of the host galaxy. Using these parameters the host galaxy flux as a function aperture radius and *FWHM* was determined assuming a Moffat $\beta = 2.5$ profile for the PSF. We have also estimated the error bars taking into account fitting errors, possible deviations from the assumed Sérsic profile and calibration errors.

The results are given in Tables B.2–B.21 in Appendix B (available online only, see Table B.1 for an example), which give the integrated fluxes of "contaminating" sources (host galaxy and significant nearby sources) as a function of aperture radius and *FWHM*. We found that the host galaxy flux depends quite strongly on the aperture radius, but *FWHM* usually has a minor effect (a few percent). We have tested the correction tables using our 4 years of monitoring data obtained at small (0.35 to 1 m) telescopes. We found the correction to work very well on average, typically we can reduce observations obtained with different aperture radii to a common aperture with an accuracy of ~1–2%. For pure nuclear fluxes the accuracy is ~5% on average, but can be over 10% in some cases.

It is important to note a few caveats with respect to the tables in Appendix B. Firstly, the results are calibrated using the comparison star data in Table 3. If a different calibration scheme is adopted, the corresponding corrections to tables in Appendix B has to be computed. Secondly, it is possible that in some sources the two dimensional fitting routine has failed to correctly separate the nuclear flux from the host galaxy flux due to deviations from a Sérsic law in the inner part of the host galaxy. Since this effect is very difficult to quantify, it has not been included in the error estimates. And thirdly, throughout this work we have assumed a Moffat $\beta = 2.5$ profile for the PSF. Real data typically present a wide variety of PSF shapes and thus our correction is not an accurate estimate in all cases. However, the tests with actual monitoring data presented here show that on average the correction works very well and it can be reliably used to subtract the host galaxy contribution, so the above effects do not change our results in any significant way.

Acknowledgements. The authors thank R. Falomo for providing deep *R*-band images for three objects. These data are partly based on observations made with the Nordic Optical Telescope, operated on the island of La Palma jointly by

Denmark, Finland, Iceland, Norway, and Sweden, in the Spanish Observatorio del Roque de los Muchachos of the Instituto de Astrofisica de Canarias. Part of the data presented here have been taken using ALFOSC, which is owned by the Instituto de Astrofisica de Andalucia (IAA) and operated at the Nordic Optical Telescope under agreement between IAA and the NBIfAFG of the Astronomical Observatory of Copenhagen.

References

Albert, J., Aliu, E., Anderhub, H., et al. 2006, ApJ, 648, L105
Bloom, S. D., & Marscher, A. P. 1996, ApJ, 461, 657
Carini, M. T., Miller, H. R., Noble, J. C., & Sadun, A. C. 1991, AJ, 101, 1196
Cellone, S. A., Romero, G. E., & Combi, J. A. 2000, ApJ, 119, 1534
Costamante, L., & Ghisellini, G. 2002, A&A, 384, 56
Cousins, A. W. J. 1984, South African Astron. Obs. Circ., 8, 69
Falomo, R. 1996, MNRAS, 283, 241
Falomo, R., & Kotilainen, J. K. 1999, A&A, 352, 85
Falomo, R., & Ulrich, M.-H. 2000, A&A, 357, 91
Falomo, R., Scarpa, R., Treves, A., & Urry, C. M. 2000, ApJ, 542, 731
Fiorucci, M., & Tosti, G. 1996, A&AS, 116, 403
Fiorucci, M., Tosti, G., & Rizzi, N. 1998, PASP, 110, 105
Fossati, G., Maraschi, L., Celotti, A., Comastri, A., & Ghisellini, G. 1998, MNRAS, 299, 433
Heidt, J., Nilsson, K., Sillanpää, A., Takalo, L. O., & Pursimo, T. 1999, A&A, 341, 683
Heidt, J., Tröller, M., Nilsson, K., et al. 2004, A&A, 418, 813
Hofmann. W., & The HESS Collaboration 2001, Proceedings of the IRCR, 2785
Howell, S. B. 1989, PASP, 101, 616
Jerzykiewicz, M., & Serkowski, K. 1966, PASP, 78, 546
Landoldt, A. U. 1983a, AJ, 88, 439
Landoldt, A. U. 1983b, AJ, 88, 853
Lorenz, E. 2004, NewAR, 48, 399
Maraschi, L., Ghisellini, G., & Celotti, A. 1992, ApJ, 397, L5
Nilsson, K., Pursimo, T., Takalo, L. O., Sillanpää, A., & Heidt, J. 1997, in Multifrequency monitoring of Blazars, Proceedings of the OJ-94 annual meeting, Perugia University Observatory, eds. G. Tosti and L. Takalo, 43
Nilsson, K., Pursimo, T., Takalo, L. O., Sillanpää, A., & Pietilä, H. 1999, PASP, 111, 1223
Nilsson, K., Pursimo, T., Heidt, J., et al. 2003, A&A, 400, 95
O'Dowd, M., & Urry, C. M. 2005, ApJ, 627, 97
Oja, T. 1996, Baltic Astron., 5, 103
Pursimo, T., Nilsson, K., Takalo, L. O., et al. 2002, A&A, 381, 810
Scarpa, R., Urry, C. M., Falomo, R., Pesce, J. E., & Treves, A. 2000a, ApJ, 532, 740
Scarpa, R., Urry, C. M., Padovani, P., Calzetti, D., & O'Dowd, M. 2000b, ApJ, 544, 258
Scorza, C., & Bender, R. 1995, A&A, 293 20
Smith, P. S., Jannuzi, B. T., & Elston, R. 1991, ApJS, 77, 67
Stickel, M., Fried, J. W., & Kühr, H. 1993, A&AS, 98, 393
Taylor, B. J. 1986, ApJS, 60, 577
Taylor, B. J., & Joner, M. D. 1985, AJ, 90, 479
Taylor, B. J., Joner, M. D., & Johnson, S. B. 1989, AJ, 97, 1798
Trujillo, I., Erwin, P., Ramos, A. A., & Graham, W. 2004, AJ, 127, 1917
Urry, C. M., & Padovani, P. 1995, PASP, 107, 803
Urry, C. M., Falomo, R., Scarpa, R., et al. 1998, ApJ, 512, 88
Urry, C. M., Scarpa, R., O'Dowd, M., et al. 2000, ApJ, 532, 816
Villata, M., Raiteri, C. M., Lanteri, L., Sobrito, G., & Cavallone, M. 1998, A&AS, 130, 305

Online Material

Appendix A: New comparison star sequences

We have calibrated new comparison star sequences for previously uncalibrated fields using the 1.03 m telescope at Tuorla Observatory during 7 photometric nights in 2003-05. The observations were made through V- and (Cousins) R-band filters using a Santa Barbara ST-1001E CCD-camera with a gain factor of 3.1 e^- ADU^{-1} and a readout noise of 17 e^-. Finding charts of the new comparison stars can be found in Fig. A.1.

During each night several BL Lac fields were observed together with 10–15 bright northern photometric standard stars from Cousins (1984); Jerzykiewicz & Serkowski (1966); Landolt (1983a; 1983b); Oja (1996); Taylor (1986); Taylor & Joner (1985) and Taylor et al. (1989). The observed frames were bias- and dark-subtracted and flat-fielded in a standard manner and instrumental magnitudes of the BL Lac comparison stars and the standard stars were determined using aperture photometry.

To determine the transformation from instrumental to standard magnitudes we fitted the standard star observations with the formulae

$$R = r + \zeta_R + k_R X + \epsilon(V - R)$$

$$V - R = \zeta_{VR} + k_{VR} X + \psi(v - r) \, ,$$

where V and R are standard magnitudes, v and r instrumental magnitudes, ζ is the zero point, k the first-order extinction coefficient, ϵ and ψ the color terms and X the airmass. The range of values found for k_R and k_{VR} were 0.10–0.15 and 0.05–0.09, respectively. The color terms were found to be stable over the whole observing period with average and rms scatter of 0.050 ± 0.011 (ϵ) and 0.77 ± 0.03 (ψ). After the fitting the comparison star magnitudes were transformed to the standard system using the adopted transformation constants. Table A.1 gives the resulting magnitudes.

To check if any of the comparison stars are variable, we have analyzed our 4 years of differential photometry of all stars in Table A.1. Our initial analysis showed that the brightnesses of all comparison stars in Table A.1 appear to be constant over the whole 4 year period with a average scatter of 1.6% (min. 0.6%, max 3.6%) around the mean level. To test the variability further we use the χ^2 statistic

$$\chi^2 = \sum_{i=0}^{N} \frac{(\overline{x}_i - \mu)^2}{\sigma_i^2} \, ,$$

where μ is the average flux of the star, $\overline{x}_i$ is the weighted average of each star during one night

$$\overline{x}_i = \frac{\sum_j x_j/\sigma_j^2}{\sum_j 1/\sigma_j^2}$$

and the corresponding error is

$$\sigma_i^2 = \frac{1}{\sum_j 1/\sigma_j^2}.$$

In the above summations j runs over one observing night and i over all observing nights. The error bars σ_j were computed by taking into account three terms: photon noise of the object, sky noise in the measurement aperture and background determination error. We further added 1.5% in square to each σ_i to take into account flat-fielding errors caused by scattered light in the telescope.

Table A.1. Comparison star magnitudes. The third column gives the number of observations for each star.

Object	Star	N_{obs}	R	$V-R$
1ES 0033+595	A	3	14.10 ± 0.03	1.06 ± 0.04
1ES 0033+595	B	3	13.33 ± 0.02	0.56 ± 0.03
1ES 0033+595	C	2	12.52 ± 0.03	0.74 ± 0.04
1ES 0033+595	D	3	13.66 ± 0.03	1.46 ± 0.04
1ES 0033+595	E	3	13.91 ± 0.02	0.55 ± 0.04
1ES 0033+595	F	3	16.67 ± 0.03	0.87 ± 0.07
1ES 0120+340	A	2	13.13 ± 0.03	0.50 ± 0.05
1ES 0120+340	B	2	13.74 ± 0.03	0.48 ± 0.05
1ES 0120+340	C	2	13.12 ± 0.03	0.38 ± 0.05
1ES 0120+340	D	2	14.02 ± 0.03	0.51 ± 0.05
1ES 0120+340	E	2	13.55 ± 0.03	0.56 ± 0.05
1ES 0120+340	F	2	16.76 ± 0.04	0.57 ± 0.07
1ES 0120+340	G	1	16.43 ± 0.04	0.45 ± 0.08
RGB J0136+391	A	3	13.13 ± 0.02	0.60 ± 0.04
RGB J0136+391	B	3	13.82 ± 0.02	0.42 ± 0.04
RGB J0136+391	C	3	14.40 ± 0.03	0.76 ± 0.04
RGB J0136+391	D	3	14.42 ± 0.03	0.46 ± 0.04
RGB J0136+391	E	3	14.84 ± 0.03	0.51 ± 0.04
RGB J0214+517	A	1	13.85 ± 0.05	0.51 ± 0.06
RGB J0214+517	B	1	14.54 ± 0.05	0.57 ± 0.06
RGB J0214+517	C	1	13.61 ± 0.05	0.38 ± 0.06
RGB J0214+517	D	1	15.09 ± 0.05	0.47 ± 0.07
RGB J0214+517	E	1	15.19 ± 0.05	0.44 ± 0.07
1ES 0647+250	A	1	13.83 ± 0.04	0.33 ± 0.05
1ES 0647+250	B	1	15.22 ± 0.04	0.38 ± 0.06
1ES 0647+250	C	1	13.40 ± 0.04	0.40 ± 0.05
1ES 0647+250	D	1	13.44 ± 0.04	0.34 ± 0.05
1ES 0647+250	E	1	13.03 ± 0.04	0.59 ± 0.05
1ES 0647+250	F	1	14.89 ± 0.04	0.38 ± 0.05
1ES 1011+496	A	3	13.40 ± 0.03	0.47 ± 0.03
1ES 1011+496	B	3	15.44 ± 0.03	0.44 ± 0.04
1ES 1011+496	C	3	15.42 ± 0.03	0.31 ± 0.04
1ES 1011+496	D	3	14.01 ± 0.03	0.31 ± 0.03
1ES 1011+496	E	3	14.04 ± 0.03	0.39 ± 0.03
RGB J1117+202	A	2	11.90 ± 0.04	0.38 ± 0.04
RGB J1117+202	B	2	12.02 ± 0.04	0.38 ± 0.04
RGB J1117+202	D	2	14.82 ± 0.04	0.70 ± 0.05
RGB J1117+202	E	2	13.56 ± 0.04	0.42 ± 0.04
RGB J1117+202	F	2	15.16 ± 0.04	0.43 ± 0.05
RGB J1136+676	A	1	14.48 ± 0.04	0.66 ± 0.06
RGB J1136+676	B	1	14.22 ± 0.04	0.48 ± 0.05
RGB J1136+676	C	1	14.73 ± 0.04	0.34 ± 0.05
RGB J1136+676	D	1	14.58 ± 0.04	0.46 ± 0.05
RGB J1136+676	E	1	15.80 ± 0.04	0.42 ± 0.07
1ES 1544+820	A	3	14.59 ± 0.03	0.37 ± 0.04
1ES 1544+820	B	3	15.35 ± 0.03	0.80 ± 0.05
1ES 1544+820	C	3	14.41 ± 0.03	0.38 ± 0.04
1ES 1544+820	D	3	12.87 ± 0.03	0.31 ± 0.04
1ES 1544+820	E	3	14.24 ± 0.03	0.41 ± 0.04

Our null hypothesis is that the flux is constant and we formally define a star variable if the null hypothesis can be rejected with $p < 0.1\%$ using the above statistic. Computing the χ^2 and its significance for each star we found that none of the stars shows significant variability. Taking into account our typical error bars we can thus conclude that any variability of these stars

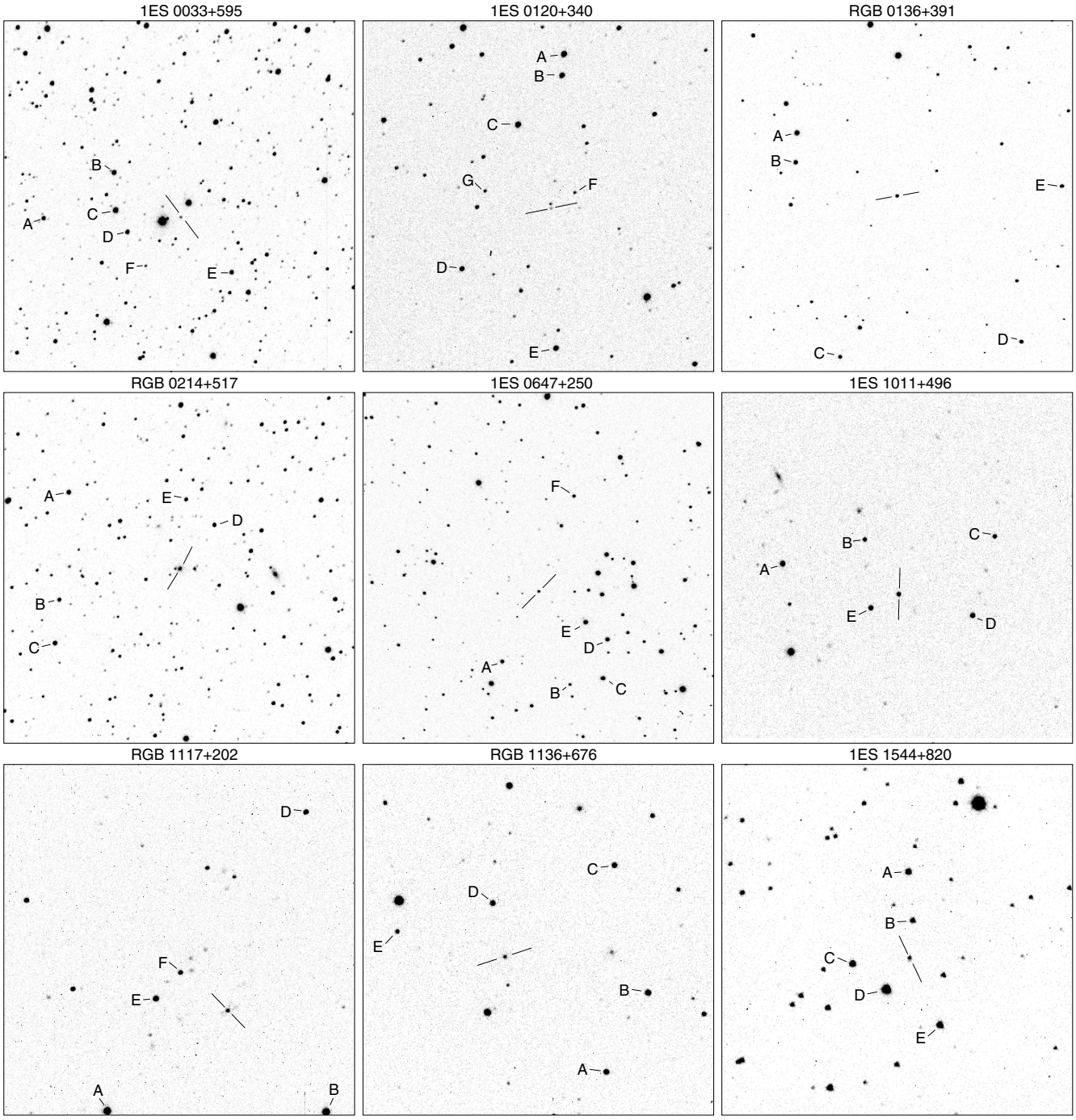

Fig. A.1. Finding charts for the new comparison star sequences. North is up and east is to the left in all images. The field size is 8 arcmin.

must be below 2–4% level, the exact value depending on the brightness of the star.

Appendix B: Host galaxy fluxes

The tables here (available online only) give the total contaminating fluxes (host galaxy + nearby companions) in mJy as a function of aperture radius and *FWHM*. The *R*-band magnitudes have been converted to linear fluxes F (Jy) using the formula $F = 3080.0 \times 10^{-0.4*R}$. Table B.1 gives an example. Note that data is shown only for aperture radii and *FWHM* larger than the resolution of the deep *R*-band images. The values have not been corrected for galactic absorption and no *K*-correction has been applied. The procedure used to derive the error bars (1σ) is explained in Sect. 4.1.

Table B.1. The contaminating fluxes (host galaxy + nearby companions) of Mrk 501 in mJy. See Table 2 for details on the photometric components included in the model.

Aperture radius (arcsec)	*FWHM* (arcsec)							
	1.0	2.0	3.0	4.0	5.0	6.0	7.0	8.0
1.0	3.4 ± 0.2	4.1 ± 0.2	5.1 ± 0.2	6.0 ± 0.2	6.8 ± 0.2	7.5 ± 0.2	8.2 ± 0.2	8.9 ± 0.2
1.5	4.4 ± 0.2	4.8 ± 0.2	5.5 ± 0.2	6.3 ± 0.2	7.0 ± 0.2	7.7 ± 0.2	8.4 ± 0.2	9.0 ± 0.2
2.0	5.3 ± 0.2	5.5 ± 0.2	6.0 ± 0.2	6.6 ± 0.2	7.3 ± 0.2	7.9 ± 0.2	8.6 ± 0.2	9.2 ± 0.2
2.5	6.2 ± 0.2	6.2 ± 0.2	6.6 ± 0.2	7.1 ± 0.2	7.6 ± 0.2	8.2 ± 0.2	8.8 ± 0.2	9.3 ± 0.2
3.0	7.1 ± 0.2	7.0 ± 0.2	7.2 ± 0.2	7.5 ± 0.2	8.0 ± 0.2	8.5 ± 0.2	9.0 ± 0.2	9.5 ± 0.2
3.5	7.8 ± 0.2	7.7 ± 0.2	7.8 ± 0.2	8.0 ± 0.2	8.4 ± 0.2	8.8 ± 0.2	9.3 ± 0.2	9.8 ± 0.2
4.0	8.5 ± 0.2	8.4 ± 0.2	8.4 ± 0.2	8.5 ± 0.2	8.8 ± 0.2	9.2 ± 0.2	9.6 ± 0.2	10.0 ± 0.3
4.5	9.2 ± 0.2	9.0 ± 0.2	8.9 ± 0.2	9.1 ± 0.2	9.3 ± 0.2	9.6 ± 0.2	9.9 ± 0.3	10.3 ± 0.3
5.0	9.8 ± 0.3	9.6 ± 0.2	9.5 ± 0.2	9.6 ± 0.2	9.7 ± 0.2	10.0 ± 0.3	10.3 ± 0.3	10.6 ± 0.3
5.5	10.3 ± 0.3	10.2 ± 0.3	10.1 ± 0.3	10.1 ± 0.3	10.2 ± 0.3	10.4 ± 0.3	10.6 ± 0.3	10.9 ± 0.3
6.0	10.9 ± 0.3	10.7 ± 0.3	10.6 ± 0.3	10.6 ± 0.3	10.6 ± 0.3	10.8 ± 0.3	11.0 ± 0.3	11.2 ± 0.3
6.5	11.4 ± 0.3	11.2 ± 0.3	11.1 ± 0.3	11.0 ± 0.3	11.1 ± 0.3	11.2 ± 0.3	11.3 ± 0.3	11.6 ± 0.3
7.0	11.8 ± 0.3	11.7 ± 0.3	11.6 ± 0.3	11.5 ± 0.3	11.5 ± 0.3	11.6 ± 0.3	11.7 ± 0.3	11.9 ± 0.3
7.5	12.3 ± 0.3	12.2 ± 0.3	12.0 ± 0.3	12.0 ± 0.3	11.9 ± 0.3	12.0 ± 0.3	12.1 ± 0.3	12.2 ± 0.3
8.0	12.7 ± 0.3	12.6 ± 0.3	12.5 ± 0.3	12.4 ± 0.3	12.3 ± 0.3	12.4 ± 0.3	12.4 ± 0.3	12.6 ± 0.3
8.5	13.2 ± 0.3	13.0 ± 0.3	12.9 ± 0.3	12.8 ± 0.3	12.8 ± 0.3	12.7 ± 0.3	12.8 ± 0.3	12.9 ± 0.3
9.0	13.6 ± 0.3	13.5 ± 0.3	13.3 ± 0.3	13.2 ± 0.3	13.1 ± 0.3	13.1 ± 0.3	13.2 ± 0.3	13.2 ± 0.3
9.5	14.0 ± 0.3	13.8 ± 0.3	13.7 ± 0.3	13.6 ± 0.3	13.5 ± 0.3	13.5 ± 0.3	13.5 ± 0.3	13.6 ± 0.3
10.0	14.3 ± 0.4	14.2 ± 0.3	14.1 ± 0.3	14.0 ± 0.3	13.9 ± 0.3	13.9 ± 0.3	13.8 ± 0.3	13.9 ± 0.3

Table B.2. The contaminating fluxes (host galaxy + nearby companions) of 1ES 0033+595 in mJy.

Aperture radius (arcsec)	*FWHM* (arcsec)						
	2.0	3.0	4.0	5.0	6.0	7.0	8.0
1.5	0.19 ± 0.01	0.19 ± 0.01	0.20 ± 0.01	0.20 ± 0.02	0.21 ± 0.02	0.21 ± 0.02	0.21 ± 0.03
2.0	0.20 ± 0.01	0.20 ± 0.01	0.20 ± 0.02	0.21 ± 0.02	0.21 ± 0.02	0.21 ± 0.02	0.21 ± 0.03
2.5	0.21 ± 0.01	0.21 ± 0.01	0.21 ± 0.02	0.21 ± 0.02	0.21 ± 0.02	0.21 ± 0.02	0.21 ± 0.03
3.0	0.21 ± 0.02	0.21 ± 0.02	0.21 ± 0.02	0.21 ± 0.02	0.21 ± 0.02	0.21 ± 0.03	0.21 ± 0.03
3.5	0.21 ± 0.02	0.21 ± 0.02	0.21 ± 0.02	0.21 ± 0.02	0.21 ± 0.02	0.21 ± 0.03	0.21 ± 0.03
4.0	0.21 ± 0.02	0.21 ± 0.02	0.21 ± 0.02	0.21 ± 0.02	0.21 ± 0.03	0.21 ± 0.03	0.21 ± 0.03
4.5	0.22 ± 0.02	0.21 ± 0.02	0.21 ± 0.03	0.21 ± 0.03	0.21 ± 0.03	0.21 ± 0.03	0.21 ± 0.03
5.0	0.22 ± 0.03	0.22 ± 0.03	0.21 ± 0.03	0.21 ± 0.03	0.21 ± 0.03	0.21 ± 0.03	0.21 ± 0.03
5.5	0.22 ± 0.03	0.22 ± 0.03	0.22 ± 0.03	0.21 ± 0.03	0.21 ± 0.03	0.21 ± 0.03	0.21 ± 0.03
6.0	0.22 ± 0.03	0.22 ± 0.03	0.22 ± 0.03	0.22 ± 0.03	0.21 ± 0.03	0.21 ± 0.03	0.21 ± 0.03
6.5	0.22 ± 0.03	0.22 ± 0.03	0.22 ± 0.03	0.22 ± 0.03	0.22 ± 0.04	0.21 ± 0.04	0.21 ± 0.04
7.0	0.22 ± 0.04	0.22 ± 0.04	0.22 ± 0.04	0.22 ± 0.04	0.22 ± 0.04	0.22 ± 0.04	0.22 ± 0.04
7.5	0.22 ± 0.04	0.22 ± 0.04	0.22 ± 0.04	0.22 ± 0.04	0.22 ± 0.04	0.22 ± 0.04	0.22 ± 0.04
8.0	0.22 ± 0.04	0.22 ± 0.04	0.22 ± 0.04	0.22 ± 0.04	0.22 ± 0.04	0.22 ± 0.04	0.22 ± 0.04
8.5	0.22 ± 0.04	0.22 ± 0.04	0.22 ± 0.04	0.22 ± 0.04	0.22 ± 0.04	0.22 ± 0.04	0.22 ± 0.04
9.0	0.22 ± 0.05	0.22 ± 0.05	0.22 ± 0.04	0.22 ± 0.04	0.22 ± 0.04	0.22 ± 0.04	0.22 ± 0.04
9.5	0.22 ± 0.05	0.22 ± 0.05	0.22 ± 0.04	0.22 ± 0.04	0.22 ± 0.04	0.22 ± 0.04	0.22 ± 0.04
10.0	0.22 ± 0.05	0.22 ± 0.05	0.22 ± 0.04	0.22 ± 0.04	0.22 ± 0.04	0.22 ± 0.04	0.22 ± 0.04

Table B.3. The contaminating fluxes (host galaxy + nearby companions) of 1ES 0120+340 in mJy.

Aperture radius (arcsec)	*FWHM* (arcsec)						
	2.0	3.0	4.0	5.0	6.0	7.0	8.0
1.5	0.10 ± 0.01	0.11 ± 0.01	0.13 ± 0.01	0.15 ± 0.01	0.18 ± 0.01	0.21 ± 0.01	0.24 ± 0.01
2.0	0.11 ± 0.01	0.12 ± 0.01	0.14 ± 0.01	0.16 ± 0.01	0.19 ± 0.01	0.22 ± 0.01	0.25 ± 0.01
2.5	0.12 ± 0.01	0.13 ± 0.01	0.14 ± 0.01	0.17 ± 0.01	0.20 ± 0.01	0.23 ± 0.01	0.26 ± 0.01
3.0	0.13 ± 0.01	0.14 ± 0.01	0.16 ± 0.01	0.18 ± 0.01	0.21 ± 0.01	0.24 ± 0.01	0.27 ± 0.01
3.5	0.14 ± 0.01	0.15 ± 0.01	0.17 ± 0.01	0.20 ± 0.01	0.22 ± 0.01	0.25 ± 0.01	0.28 ± 0.01
4.0	0.15 ± 0.01	0.17 ± 0.01	0.19 ± 0.01	0.22 ± 0.01	0.24 ± 0.01	0.27 ± 0.01	0.30 ± 0.01
4.5	0.17 ± 0.01	0.19 ± 0.01	0.21 ± 0.01	0.24 ± 0.01	0.26 ± 0.01	0.29 ± 0.01	0.31 ± 0.01
5.0	0.19 ± 0.01	0.22 ± 0.01	0.24 ± 0.01	0.27 ± 0.01	0.29 ± 0.01	0.31 ± 0.01	0.33 ± 0.01
5.5	0.23 ± 0.01	0.26 ± 0.01	0.28 ± 0.01	0.30 ± 0.01	0.31 ± 0.01	0.33 ± 0.01	0.35 ± 0.01
6.0	0.29 ± 0.01	0.31 ± 0.01	0.32 ± 0.01	0.33 ± 0.01	0.34 ± 0.01	0.36 ± 0.01	0.37 ± 0.01
6.5	0.37 ± 0.01	0.36 ± 0.01	0.36 ± 0.01	0.37 ± 0.01	0.37 ± 0.01	0.38 ± 0.01	0.39 ± 0.01
7.0	0.45 ± 0.02	0.42 ± 0.01	0.41 ± 0.01	0.40 ± 0.01	0.40 ± 0.01	0.41 ± 0.01	0.41 ± 0.01
7.5	0.51 ± 0.02	0.47 ± 0.02	0.45 ± 0.01	0.44 ± 0.01	0.43 ± 0.01	0.43 ± 0.01	0.43 ± 0.01
8.0	0.55 ± 0.02	0.51 ± 0.02	0.48 ± 0.02	0.47 ± 0.02	0.46 ± 0.02	0.45 ± 0.02	0.45 ± 0.02
8.5	0.57 ± 0.02	0.54 ± 0.02	0.51 ± 0.02	0.49 ± 0.02	0.48 ± 0.02	0.48 ± 0.02	0.47 ± 0.02
9.0	0.59 ± 0.02	0.56 ± 0.02	0.54 ± 0.02	0.52 ± 0.02	0.50 ± 0.02	0.49 ± 0.02	0.49 ± 0.02
9.5	0.60 ± 0.02	0.58 ± 0.02	0.55 ± 0.02	0.54 ± 0.02	0.52 ± 0.02	0.51 ± 0.02	0.51 ± 0.02
10.0	0.60 ± 0.02	0.59 ± 0.02	0.57 ± 0.02	0.55 ± 0.02	0.54 ± 0.02	0.53 ± 0.02	0.52 ± 0.02

Table B.4. The contaminating fluxes (host galaxy + nearby companions) of RGB J0214+517 in mJy.

Aperture radius (arcsec)	*FWHM* (arcsec)							
	1.0	2.0	3.0	4.0	5.0	6.0	7.0	8.0
1.0	0.72 ± 0.03	0.89 ± 0.03	1.09 ± 0.04	1.29 ± 0.04	1.47 ± 0.05	1.65 ± 0.05	1.82 ± 0.06	1.97 ± 0.06
1.5	0.94 ± 0.04	1.03 ± 0.04	1.18 ± 0.04	1.35 ± 0.05	1.52 ± 0.05	1.69 ± 0.05	1.85 ± 0.06	2.01 ± 0.06
2.0	1.15 ± 0.04	1.18 ± 0.04	1.29 ± 0.04	1.44 ± 0.05	1.59 ± 0.05	1.75 ± 0.06	1.90 ± 0.06	2.05 ± 0.06
2.5	1.34 ± 0.05	1.34 ± 0.05	1.42 ± 0.05	1.53 ± 0.05	1.67 ± 0.05	1.81 ± 0.06	1.95 ± 0.06	2.09 ± 0.07
3.0	1.51 ± 0.05	1.50 ± 0.05	1.54 ± 0.05	1.64 ± 0.05	1.75 ± 0.06	1.88 ± 0.06	2.01 ± 0.06	2.14 ± 0.07
3.5	1.67 ± 0.06	1.65 ± 0.05	1.68 ± 0.05	1.75 ± 0.06	1.85 ± 0.06	1.96 ± 0.06	2.08 ± 0.06	2.20 ± 0.07
4.0	1.81 ± 0.06	1.79 ± 0.06	1.82 ± 0.06	1.87 ± 0.06	1.96 ± 0.06	2.05 ± 0.06	2.16 ± 0.07	2.26 ± 0.07
4.5	1.95 ± 0.06	1.94 ± 0.06	1.96 ± 0.06	2.00 ± 0.06	2.07 ± 0.06	2.15 ± 0.07	2.24 ± 0.07	2.33 ± 0.07
5.0	2.08 ± 0.07	2.09 ± 0.07	2.10 ± 0.07	2.13 ± 0.07	2.18 ± 0.07	2.25 ± 0.07	2.32 ± 0.07	2.40 ± 0.08
5.5	2.24 ± 0.07	2.25 ± 0.07	2.25 ± 0.07	2.27 ± 0.07	2.30 ± 0.07	2.35 ± 0.07	2.41 ± 0.07	2.48 ± 0.08
6.0	2.45 ± 0.08	2.43 ± 0.08	2.41 ± 0.07	2.40 ± 0.07	2.42 ± 0.07	2.45 ± 0.08	2.50 ± 0.08	2.56 ± 0.08
6.5	2.69 ± 0.08	2.61 ± 0.08	2.56 ± 0.08	2.54 ± 0.08	2.54 ± 0.08	2.56 ± 0.08	2.60 ± 0.08	2.64 ± 0.08
7.0	2.86 ± 0.09	2.76 ± 0.08	2.70 ± 0.08	2.66 ± 0.08	2.65 ± 0.08	2.66 ± 0.08	2.69 ± 0.08	2.72 ± 0.09
7.5	2.97 ± 0.09	2.90 ± 0.09	2.83 ± 0.09	2.79 ± 0.08	2.76 ± 0.08	2.76 ± 0.08	2.78 ± 0.09	2.81 ± 0.09
8.0	3.06 ± 0.09	3.01 ± 0.09	2.94 ± 0.09	2.90 ± 0.09	2.87 ± 0.09	2.86 ± 0.09	2.87 ± 0.09	2.9 ± 0.1
8.5	3.15 ± 0.09	3.10 ± 0.09	3.05 ± 0.09	3.00 ± 0.09	2.97 ± 0.09	2.95 ± 0.09	3.0 ± 0.1	3.0 ± 0.1
9.0	3.2 ± 0.1	3.2 ± 0.1	3.14 ± 0.09	3.09 ± 0.09	3.06 ± 0.09	3.0 ± 0.1	3.0 ± 0.1	3.0 ± 0.2
9.5	3.3 ± 0.1	3.3 ± 0.1	3.2 ± 0.1	3.2 ± 0.1	3.2 ± 0.1	3.1 ± 0.1	3.1 ± 0.1	3.1 ± 0.2
10.0	3.4 ± 0.1	3.3 ± 0.1	3.3 ± 0.1	3.3 ± 0.1	3.2 ± 0.1	3.2 ± 0.1	3.2 ± 0.2	3.2 ± 0.2

Table B.5. The contaminating fluxes (host galaxy + nearby companions) of 1ES 0806+524 in mJy.

Aperture radius (arcsec)	*FWHM* (arcsec)							
	1.0	2.0	3.0	4.0	5.0	6.0	7.0	8.0
1.0	0.26 ± 0.04	0.31 ± 0.04	0.36 ± 0.03	0.41 ± 0.03	0.45 ± 0.03	0.49 ± 0.03	0.52 ± 0.03	0.55 ± 0.03
1.5	0.32 ± 0.04	0.35 ± 0.04	0.38 ± 0.04	0.43 ± 0.03	0.46 ± 0.03	0.50 ± 0.03	0.53 ± 0.03	0.56 ± 0.04
2.0	0.38 ± 0.04	0.39 ± 0.04	0.41 ± 0.04	0.45 ± 0.03	0.48 ± 0.03	0.51 ± 0.03	0.54 ± 0.03	0.56 ± 0.04
2.5	0.43 ± 0.04	0.43 ± 0.04	0.45 ± 0.04	0.47 ± 0.03	0.50 ± 0.03	0.52 ± 0.03	0.55 ± 0.03	0.57 ± 0.03
3.0	0.48 ± 0.04	0.47 ± 0.04	0.48 ± 0.04	0.49 ± 0.03	0.51 ± 0.03	0.54 ± 0.03	0.56 ± 0.03	0.58 ± 0.03
3.5	0.52 ± 0.04	0.51 ± 0.04	0.51 ± 0.04	0.52 ± 0.04	0.53 ± 0.04	0.55 ± 0.03	0.57 ± 0.04	0.59 ± 0.03
4.0	0.55 ± 0.04	0.54 ± 0.04	0.54 ± 0.04	0.54 ± 0.04	0.55 ± 0.04	0.57 ± 0.03	0.59 ± 0.04	0.60 ± 0.04
4.5	0.58 ± 0.04	0.57 ± 0.04	0.56 ± 0.04	0.57 ± 0.04	0.57 ± 0.04	0.59 ± 0.04	0.60 ± 0.04	0.61 ± 0.04
5.0	0.61 ± 0.04	0.60 ± 0.04	0.59 ± 0.04	0.59 ± 0.04	0.59 ± 0.04	0.60 ± 0.04	0.61 ± 0.04	0.63 ± 0.04
5.5	0.63 ± 0.04	0.62 ± 0.04	0.61 ± 0.04	0.61 ± 0.04	0.61 ± 0.04	0.62 ± 0.04	0.63 ± 0.04	0.64 ± 0.04
6.0	0.65 ± 0.04	0.64 ± 0.04	0.64 ± 0.04	0.63 ± 0.04	0.63 ± 0.04	0.64 ± 0.04	0.64 ± 0.04	0.65 ± 0.04
6.5	0.67 ± 0.05	0.66 ± 0.04	0.66 ± 0.04	0.65 ± 0.04	0.65 ± 0.04	0.65 ± 0.04	0.66 ± 0.04	0.66 ± 0.04
7.0	0.69 ± 0.05	0.68 ± 0.04	0.68 ± 0.04	0.67 ± 0.04	0.67 ± 0.04	0.67 ± 0.04	0.67 ± 0.04	0.68 ± 0.04
7.5	0.71 ± 0.05	0.70 ± 0.04	0.69 ± 0.04	0.69 ± 0.04	0.68 ± 0.04	0.68 ± 0.04	0.69 ± 0.04	0.69 ± 0.04
8.0	0.72 ± 0.05	0.72 ± 0.04	0.71 ± 0.04	0.70 ± 0.04	0.70 ± 0.04	0.70 ± 0.04	0.70 ± 0.04	0.70 ± 0.04
8.5	0.74 ± 0.05	0.73 ± 0.04	0.73 ± 0.04	0.72 ± 0.04	0.72 ± 0.04	0.71 ± 0.04	0.71 ± 0.04	0.71 ± 0.04
9.0	0.75 ± 0.05	0.75 ± 0.04	0.74 ± 0.04	0.73 ± 0.04	0.73 ± 0.04	0.73 ± 0.04	0.73 ± 0.04	0.73 ± 0.04
9.5	0.76 ± 0.05	0.76 ± 0.04	0.75 ± 0.04	0.75 ± 0.04	0.74 ± 0.04	0.74 ± 0.04	0.74 ± 0.04	0.74 ± 0.04
10.0	0.78 ± 0.05	0.77 ± 0.04	0.77 ± 0.04	0.76 ± 0.04	0.76 ± 0.04	0.75 ± 0.04	0.75 ± 0.04	0.75 ± 0.04

Table B.6. The contaminating fluxes (host galaxy + nearby companions) of 1ES 1011+496 in mJy.

Aperture radius (arcsec)	*FWHM* (arcsec)							
	1.0	2.0	3.0	4.0	5.0	6.0	7.0	8.0
1.0	0.26 ± 0.01	0.29 ± 0.01	0.32 ± 0.01	0.34 ± 0.02	0.37 ± 0.02	0.38 ± 0.02	0.40 ± 0.02	0.42 ± 0.02
1.5	0.30 ± 0.01	0.31 ± 0.01	0.33 ± 0.02	0.35 ± 0.02	0.37 ± 0.02	0.39 ± 0.02	0.41 ± 0.02	0.42 ± 0.02
2.0	0.33 ± 0.02	0.33 ± 0.02	0.35 ± 0.02	0.36 ± 0.02	0.38 ± 0.02	0.40 ± 0.02	0.41 ± 0.02	0.42 ± 0.02
2.5	0.36 ± 0.02	0.36 ± 0.02	0.36 ± 0.02	0.38 ± 0.02	0.39 ± 0.02	0.40 ± 0.02	0.42 ± 0.02	0.43 ± 0.02
3.0	0.38 ± 0.02	0.38 ± 0.02	0.38 ± 0.02	0.39 ± 0.02	0.40 ± 0.02	0.41 ± 0.02	0.42 ± 0.02	0.43 ± 0.02
3.5	0.40 ± 0.02	0.40 ± 0.02	0.40 ± 0.02	0.40 ± 0.02	0.41 ± 0.02	0.42 ± 0.02	0.43 ± 0.02	0.44 ± 0.02
4.0	0.42 ± 0.02	0.41 ± 0.02	0.41 ± 0.02	0.41 ± 0.02	0.42 ± 0.02	0.43 ± 0.02	0.43 ± 0.02	0.44 ± 0.02
4.5	0.43 ± 0.02	0.43 ± 0.02	0.42 ± 0.02	0.43 ± 0.02	0.43 ± 0.02	0.43 ± 0.02	0.44 ± 0.02	0.45 ± 0.02
5.0	0.45 ± 0.02	0.44 ± 0.02	0.44 ± 0.02	0.44 ± 0.02	0.44 ± 0.02	0.44 ± 0.02	0.45 ± 0.02	0.45 ± 0.02
5.5	0.46 ± 0.02	0.45 ± 0.02	0.45 ± 0.02	0.45 ± 0.02	0.45 ± 0.02	0.45 ± 0.02	0.46 ± 0.02	0.46 ± 0.02
6.0	0.47 ± 0.02	0.46 ± 0.02	0.46 ± 0.02	0.46 ± 0.02	0.46 ± 0.02	0.46 ± 0.02	0.46 ± 0.02	0.47 ± 0.02
6.5	0.48 ± 0.02	0.47 ± 0.02	0.47 ± 0.02	0.47 ± 0.02	0.47 ± 0.02	0.47 ± 0.02	0.47 ± 0.02	0.47 ± 0.02
7.0	0.49 ± 0.02	0.48 ± 0.02	0.48 ± 0.02	0.48 ± 0.02	0.48 ± 0.02	0.48 ± 0.02	0.48 ± 0.02	0.48 ± 0.02
7.5	0.50 ± 0.02	0.49 ± 0.02	0.49 ± 0.02	0.49 ± 0.02	0.48 ± 0.02	0.48 ± 0.02	0.48 ± 0.02	0.49 ± 0.02
8.0	0.50 ± 0.02	0.50 ± 0.02	0.50 ± 0.02	0.49 ± 0.02	0.49 ± 0.02	0.49 ± 0.02	0.49 ± 0.02	0.49 ± 0.02
8.5	0.51 ± 0.02	0.51 ± 0.02	0.50 ± 0.02	0.50 ± 0.02	0.50 ± 0.02	0.50 ± 0.02	0.50 ± 0.02	0.50 ± 0.02
9.0	0.52 ± 0.02	0.51 ± 0.02	0.51 ± 0.02	0.51 ± 0.02	0.51 ± 0.02	0.50 ± 0.02	0.50 ± 0.02	0.50 ± 0.02
9.5	0.52 ± 0.02	0.52 ± 0.02	0.52 ± 0.02	0.51 ± 0.02	0.51 ± 0.02	0.51 ± 0.02	0.51 ± 0.02	0.51 ± 0.02
10.0	0.53 ± 0.02	0.53 ± 0.02	0.52 ± 0.02	0.52 ± 0.02	0.52 ± 0.02	0.52 ± 0.02	0.52 ± 0.02	0.52 ± 0.02

Table B.7. The contaminating fluxes (host galaxy + nearby companions) of 1ES 1028+511 in mJy.

Aperture radius (arcsec)	*FWHM* (arcsec)							
	1.0	2.0	3.0	4.0	5.0	6.0	7.0	8.0
1.0	0.04 ± 0.02	0.05 ± 0.02	0.06 ± 0.02	0.06 ± 0.02	0.07 ± 0.02	0.07 ± 0.02	0.08 ± 0.02	0.08 ± 0.02
1.5	0.05 ± 0.02	0.05 ± 0.02	0.06 ± 0.02	0.07 ± 0.02	0.07 ± 0.02	0.07 ± 0.02	0.08 ± 0.02	0.08 ± 0.02
2.0	0.06 ± 0.02	0.06 ± 0.02	0.06 ± 0.02	0.07 ± 0.02	0.07 ± 0.02	0.08 ± 0.02	0.08 ± 0.02	0.08 ± 0.02
2.5	0.07 ± 0.02	0.07 ± 0.02	0.07 ± 0.02	0.07 ± 0.02	0.07 ± 0.02	0.08 ± 0.02	0.08 ± 0.02	0.08 ± 0.02
3.0	0.07 ± 0.02	0.07 ± 0.02	0.07 ± 0.02	0.07 ± 0.02	0.08 ± 0.02	0.08 ± 0.02	0.08 ± 0.02	0.08 ± 0.02
3.5	0.08 ± 0.02	0.08 ± 0.02	0.08 ± 0.02	0.08 ± 0.02	0.08 ± 0.02	0.08 ± 0.02	0.08 ± 0.02	0.08 ± 0.02
4.0	0.08 ± 0.02	0.08 ± 0.02	0.08 ± 0.02	0.08 ± 0.02	0.08 ± 0.02	0.08 ± 0.02	0.08 ± 0.02	0.09 ± 0.02
4.5	0.09 ± 0.02	0.08 ± 0.02	0.08 ± 0.02	0.08 ± 0.02	0.08 ± 0.02	0.08 ± 0.02	0.09 ± 0.02	0.09 ± 0.02
5.0	0.09 ± 0.02	0.09 ± 0.02	0.09 ± 0.02	0.09 ± 0.02	0.09 ± 0.02	0.09 ± 0.02	0.09 ± 0.02	0.09 ± 0.02
5.5	0.09 ± 0.02	0.09 ± 0.02	0.09 ± 0.02	0.09 ± 0.02	0.09 ± 0.02	0.09 ± 0.02	0.09 ± 0.02	0.09 ± 0.02
6.0	0.09 ± 0.02	0.09 ± 0.02	0.09 ± 0.02	0.09 ± 0.02	0.09 ± 0.02	0.09 ± 0.02	0.09 ± 0.02	0.09 ± 0.02
6.5	0.10 ± 0.02	0.09 ± 0.02	0.09 ± 0.02	0.09 ± 0.02	0.09 ± 0.02	0.09 ± 0.02	0.09 ± 0.02	0.09 ± 0.02
7.0	0.10 ± 0.02	0.10 ± 0.02	0.09 ± 0.02	0.09 ± 0.02	0.09 ± 0.02	0.09 ± 0.02	0.09 ± 0.02	0.09 ± 0.02
7.5	0.10 ± 0.02	0.10 ± 0.02	0.10 ± 0.02	0.10 ± 0.02	0.10 ± 0.02	0.09 ± 0.02	0.09 ± 0.02	0.09 ± 0.02
8.0	0.10 ± 0.02	0.10 ± 0.02	0.10 ± 0.02	0.10 ± 0.02	0.10 ± 0.02	0.10 ± 0.02	0.10 ± 0.02	0.10 ± 0.02
8.5	0.10 ± 0.02	0.10 ± 0.02	0.10 ± 0.02	0.10 ± 0.02	0.10 ± 0.02	0.10 ± 0.02	0.10 ± 0.01	0.10 ± 0.01
9.0	0.10 ± 0.01	0.10 ± 0.01	0.10 ± 0.01	0.10 ± 0.01	0.10 ± 0.01	0.10 ± 0.01	0.10 ± 0.01	0.10 ± 0.01
9.5	0.10 ± 0.01	0.10 ± 0.01	0.10 ± 0.01	0.10 ± 0.01	0.10 ± 0.01	0.10 ± 0.01	0.10 ± 0.01	0.10 ± 0.01
10.0	0.10 ± 0.01	0.10 ± 0.01	0.10 ± 0.01	0.10 ± 0.01	0.10 ± 0.01	0.10 ± 0.01	0.10 ± 0.01	0.10 ± 0.01

Table B.8. The contaminating fluxes (host galaxy + nearby companions) of Mrk 421 in mJy.

Aperture radius (arcsec)	*FWHM* (arcsec)							
	1.0	2.0	3.0	4.0	5.0	6.0	7.0	8.0
1.0	1.3 ± 0.2	1.8 ± 0.2	2.5 ± 0.3	3.2 ± 0.3	3.8 ± 0.3	4.4 ± 0.3	5.0 ± 0.4	5.5 ± 0.4
1.5	1.9 ± 0.3	2.2 ± 0.3	2.8 ± 0.3	3.4 ± 0.3	4.0 ± 0.3	4.5 ± 0.3	5.1 ± 0.4	5.6 ± 0.4
2.0	2.6 ± 0.3	2.7 ± 0.3	3.1 ± 0.3	3.7 ± 0.3	4.2 ± 0.3	4.7 ± 0.4	5.2 ± 0.4	5.7 ± 0.4
2.5	3.2 ± 0.4	3.3 ± 0.3	3.6 ± 0.3	4.0 ± 0.3	4.5 ± 0.3	4.9 ± 0.4	5.4 ± 0.4	5.9 ± 0.4
3.0	3.9 ± 0.4	3.9 ± 0.4	4.0 ± 0.4	4.4 ± 0.4	4.8 ± 0.4	5.2 ± 0.4	5.6 ± 0.4	6.0 ± 0.4
3.5	4.5 ± 0.4	4.4 ± 0.4	4.5 ± 0.4	4.8 ± 0.4	5.1 ± 0.4	5.5 ± 0.4	5.8 ± 0.4	6.2 ± 0.4
4.0	5.1 ± 0.4	5.0 ± 0.4	5.0 ± 0.4	5.2 ± 0.4	5.4 ± 0.4	5.7 ± 0.4	6.1 ± 0.4	6.4 ± 0.4
4.5	5.7 ± 0.4	5.5 ± 0.4	5.5 ± 0.4	5.6 ± 0.4	5.8 ± 0.4	6.1 ± 0.4	6.3 ± 0.4	6.7 ± 0.4
5.0	6.2 ± 0.4	6.0 ± 0.4	6.0 ± 0.4	6.0 ± 0.4	6.2 ± 0.4	6.4 ± 0.4	6.6 ± 0.4	6.9 ± 0.4
5.5	6.7 ± 0.4	6.5 ± 0.4	6.4 ± 0.4	6.5 ± 0.4	6.5 ± 0.4	6.7 ± 0.4	6.9 ± 0.4	7.1 ± 0.4
6.0	7.1 ± 0.4	7.0 ± 0.4	6.9 ± 0.4	6.9 ± 0.4	6.9 ± 0.4	7.0 ± 0.4	7.2 ± 0.4	7.4 ± 0.4
6.5	7.6 ± 0.4	7.4 ± 0.4	7.3 ± 0.4	7.3 ± 0.4	7.3 ± 0.4	7.4 ± 0.4	7.5 ± 0.4	7.7 ± 0.4
7.0	8.0 ± 0.4	7.8 ± 0.4	7.7 ± 0.4	7.6 ± 0.4	7.6 ± 0.4	7.7 ± 0.4	7.8 ± 0.4	7.9 ± 0.4
7.5	8.3 ± 0.4	8.2 ± 0.4	8.1 ± 0.4	8.0 ± 0.4	8.0 ± 0.4	8.0 ± 0.4	8.1 ± 0.4	8.2 ± 0.4
8.0	8.7 ± 0.4	8.6 ± 0.4	8.5 ± 0.4	8.4 ± 0.4	8.3 ± 0.4	8.3 ± 0.4	8.4 ± 0.4	8.4 ± 0.4
8.5	9.0 ± 0.4	8.9 ± 0.4	8.8 ± 0.4	8.7 ± 0.4	8.7 ± 0.4	8.6 ± 0.4	8.6 ± 0.4	8.7 ± 0.4
9.0	9.3 ± 0.4	9.2 ± 0.4	9.1 ± 0.4	9.0 ± 0.4	9.0 ± 0.4	8.9 ± 0.4	8.9 ± 0.4	8.9 ± 0.4
9.5	9.6 ± 0.4	9.6 ± 0.4	9.4 ± 0.4	9.3 ± 0.4	9.3 ± 0.4	9.2 ± 0.4	9.2 ± 0.4	9.2 ± 0.4
10.0	9.9 ± 0.5	9.8 ± 0.5	9.7 ± 0.5	9.6 ± 0.5	9.6 ± 0.5	9.5 ± 0.5	9.4 ± 0.5	9.4 ± 0.4

Table B.9. The contaminating fluxes (host galaxy + nearby companions) of RGB J1117+202 in mJy.

Aperture radius (arcsec)	*FWHM* (arcsec)							
	1.0	2.0	3.0	4.0	5.0	6.0	7.0	8.0
1.0	0.16 ± 0.03	0.20 ± 0.03	0.26 ± 0.03	0.31 ± 0.03	0.36 ± 0.03	0.40 ± 0.03	0.44 ± 0.03	0.48 ± 0.03
1.5	0.21 ± 0.03	0.24 ± 0.03	0.28 ± 0.03	0.32 ± 0.03	0.37 ± 0.03	0.41 ± 0.03	0.45 ± 0.03	0.49 ± 0.03
2.0	0.27 ± 0.03	0.28 ± 0.03	0.31 ± 0.03	0.35 ± 0.03	0.38 ± 0.03	0.42 ± 0.03	0.46 ± 0.03	0.50 ± 0.03
2.5	0.32 ± 0.03	0.32 ± 0.03	0.34 ± 0.03	0.37 ± 0.03	0.40 ± 0.03	0.44 ± 0.03	0.47 ± 0.03	0.51 ± 0.03
3.0	0.37 ± 0.03	0.36 ± 0.03	0.37 ± 0.03	0.40 ± 0.03	0.42 ± 0.03	0.46 ± 0.03	0.49 ± 0.03	0.52 ± 0.03
3.5	0.41 ± 0.03	0.40 ± 0.03	0.41 ± 0.03	0.42 ± 0.03	0.45 ± 0.03	0.47 ± 0.03	0.51 ± 0.03	0.54 ± 0.03
4.0	0.45 ± 0.03	0.44 ± 0.03	0.44 ± 0.03	0.45 ± 0.03	0.47 ± 0.03	0.50 ± 0.03	0.52 ± 0.03	0.55 ± 0.03
4.5	0.49 ± 0.03	0.48 ± 0.03	0.47 ± 0.03	0.48 ± 0.03	0.50 ± 0.03	0.52 ± 0.03	0.54 ± 0.03	0.57 ± 0.03
5.0	0.52 ± 0.03	0.51 ± 0.03	0.51 ± 0.03	0.51 ± 0.03	0.52 ± 0.03	0.54 ± 0.03	0.57 ± 0.03	0.59 ± 0.03
5.5	0.55 ± 0.03	0.54 ± 0.03	0.54 ± 0.03	0.54 ± 0.03	0.55 ± 0.03	0.57 ± 0.03	0.59 ± 0.03	0.61 ± 0.04
6.0	0.57 ± 0.03	0.57 ± 0.03	0.57 ± 0.03	0.57 ± 0.03	0.58 ± 0.03	0.59 ± 0.03	0.61 ± 0.04	0.63 ± 0.04
6.5	0.60 ± 0.03	0.60 ± 0.03	0.60 ± 0.03	0.60 ± 0.03	0.61 ± 0.03	0.62 ± 0.04	0.64 ± 0.04	0.66 ± 0.04
7.0	0.63 ± 0.04	0.63 ± 0.04	0.63 ± 0.04	0.63 ± 0.04	0.64 ± 0.04	0.65 ± 0.04	0.66 ± 0.04	0.68 ± 0.04
7.5	0.65 ± 0.04	0.66 ± 0.04	0.66 ± 0.04	0.66 ± 0.04	0.67 ± 0.04	0.68 ± 0.04	0.69 ± 0.04	0.71 ± 0.04
8.0	0.68 ± 0.04	0.69 ± 0.04	0.69 ± 0.04	0.70 ± 0.04	0.70 ± 0.04	0.71 ± 0.04	0.72 ± 0.04	0.73 ± 0.04
8.5	0.72 ± 0.04	0.73 ± 0.04	0.73 ± 0.04	0.73 ± 0.04	0.73 ± 0.04	0.74 ± 0.04	0.75 ± 0.04	0.76 ± 0.04
9.0	0.77 ± 0.04	0.77 ± 0.04	0.77 ± 0.04	0.77 ± 0.04	0.77 ± 0.04	0.77 ± 0.04	0.78 ± 0.04	0.78 ± 0.04
9.5	0.82 ± 0.04	0.81 ± 0.04	0.81 ± 0.04	0.80 ± 0.04	0.80 ± 0.04	0.80 ± 0.04	0.81 ± 0.04	0.81 ± 0.04
10.0	0.86 ± 0.04	0.85 ± 0.04	0.85 ± 0.04	0.84 ± 0.04	0.84 ± 0.04	0.84 ± 0.04	0.84 ± 0.04	0.84 ± 0.04

Table B.10. The contaminating fluxes (host galaxy + nearby companions) of Mrk 180 in mJy.

Aperture radius (arcsec)	*FWHM* (arcsec)						
	2.0	3.0	4.0	5.0	6.0	7.0	8.0
1.5	1.29 ± 0.06	1.53 ± 0.07	1.82 ± 0.08	2.14 ± 0.09	2.5 ± 0.1	2.8 ± 0.2	3.1 ± 0.2
2.0	1.52 ± 0.07	1.70 ± 0.07	1.96 ± 0.08	2.26 ± 0.09	2.6 ± 0.2	2.9 ± 0.2	3.2 ± 0.2
2.5	1.75 ± 0.07	1.89 ± 0.08	2.12 ± 0.09	2.4 ± 0.1	2.7 ± 0.2	3.0 ± 0.2	3.3 ± 0.2
3.0	1.98 ± 0.08	2.09 ± 0.09	2.3 ± 0.1	2.6 ± 0.2	2.8 ± 0.2	3.1 ± 0.2	3.4 ± 0.2
3.5	2.22 ± 0.09	2.3 ± 0.1	2.5 ± 0.1	2.7 ± 0.2	3.0 ± 0.2	3.3 ± 0.2	3.6 ± 0.2
4.0	2.4 ± 0.1	2.6 ± 0.2	2.7 ± 0.2	3.0 ± 0.2	3.2 ± 0.2	3.5 ± 0.2	3.7 ± 0.2
4.5	2.7 ± 0.2	2.8 ± 0.2	3.0 ± 0.2	3.2 ± 0.2	3.4 ± 0.2	3.7 ± 0.2	3.9 ± 0.2
5.0	3.0 ± 0.2	3.2 ± 0.2	3.3 ± 0.2	3.5 ± 0.2	3.7 ± 0.2	3.9 ± 0.2	4.1 ± 0.2
5.5	3.4 ± 0.2	3.5 ± 0.2	3.6 ± 0.2	3.8 ± 0.2	3.9 ± 0.2	4.1 ± 0.2	4.2 ± 0.2
6.0	3.9 ± 0.2	4.0 ± 0.2	4.0 ± 0.2	4.1 ± 0.2	4.2 ± 0.2	4.3 ± 0.2	4.4 ± 0.2
6.5	4.5 ± 0.2	4.4 ± 0.2	4.4 ± 0.2	4.4 ± 0.2	4.4 ± 0.2	4.5 ± 0.2	4.6 ± 0.2
7.0	5.1 ± 0.2	4.8 ± 0.2	4.7 ± 0.2	4.7 ± 0.2	4.7 ± 0.2	4.8 ± 0.2	4.8 ± 0.2
7.5	5.5 ± 0.3	5.2 ± 0.3	5.1 ± 0.2	5.0 ± 0.2	5.0 ± 0.2	5.0 ± 0.2	5.0 ± 0.2
8.0	5.8 ± 0.3	5.6 ± 0.3	5.4 ± 0.3	5.3 ± 0.3	5.2 ± 0.3	5.2 ± 0.2	5.2 ± 0.3
8.5	6.1 ± 0.3	5.8 ± 0.3	5.6 ± 0.3	5.5 ± 0.3	5.4 ± 0.3	5.4 ± 0.3	5.4 ± 0.3
9.0	6.2 ± 0.3	6.0 ± 0.3	5.9 ± 0.3	5.7 ± 0.3	5.6 ± 0.3	5.6 ± 0.3	5.6 ± 0.3
9.5	6.4 ± 0.3	6.2 ± 0.3	6.1 ± 0.3	5.9 ± 0.3	5.8 ± 0.3	5.8 ± 0.3	5.8 ± 0.3
10.0	6.5 ± 0.3	6.4 ± 0.3	6.2 ± 0.3	6.1 ± 0.3	6.0 ± 0.3	5.9 ± 0.3	5.9 ± 0.3

Table B.11. The contaminating fluxes (host galaxy + nearby companions) of RGB J1136+676 in mJy.

Aperture radius (arcsec)	*FWHM* (arcsec)							
	1.0	2.0	3.0	4.0	5.0	6.0	7.0	8.0
1.0	0.30 ± 0.02	0.36 ± 0.02	0.43 ± 0.02	0.49 ± 0.02	0.54 ± 0.03	0.59 ± 0.03	0.63 ± 0.03	0.67 ± 0.03
1.5	0.38 ± 0.02	0.41 ± 0.02	0.46 ± 0.02	0.51 ± 0.03	0.56 ± 0.03	0.60 ± 0.03	0.64 ± 0.03	0.67 ± 0.03
2.0	0.46 ± 0.02	0.46 ± 0.02	0.50 ± 0.03	0.54 ± 0.03	0.58 ± 0.03	0.62 ± 0.03	0.65 ± 0.03	0.69 ± 0.03
2.5	0.52 ± 0.03	0.52 ± 0.03	0.53 ± 0.03	0.56 ± 0.03	0.60 ± 0.03	0.63 ± 0.03	0.66 ± 0.03	0.70 ± 0.03
3.0	0.57 ± 0.03	0.56 ± 0.03	0.57 ± 0.03	0.59 ± 0.03	0.62 ± 0.03	0.65 ± 0.03	0.68 ± 0.03	0.71 ± 0.03
3.5	0.62 ± 0.03	0.61 ± 0.03	0.61 ± 0.03	0.62 ± 0.03	0.64 ± 0.03	0.67 ± 0.03	0.69 ± 0.03	0.72 ± 0.03
4.0	0.66 ± 0.03	0.65 ± 0.03	0.65 ± 0.03	0.65 ± 0.03	0.67 ± 0.03	0.69 ± 0.03	0.71 ± 0.03	0.74 ± 0.03
4.5	0.70 ± 0.03	0.69 ± 0.03	0.68 ± 0.03	0.69 ± 0.03	0.70 ± 0.03	0.71 ± 0.03	0.73 ± 0.03	0.75 ± 0.04
5.0	0.73 ± 0.03	0.72 ± 0.03	0.71 ± 0.03	0.71 ± 0.03	0.72 ± 0.03	0.73 ± 0.03	0.75 ± 0.04	0.77 ± 0.04
5.5	0.76 ± 0.04	0.75 ± 0.04	0.74 ± 0.03	0.74 ± 0.03	0.75 ± 0.03	0.76 ± 0.04	0.77 ± 0.04	0.78 ± 0.04
6.0	0.79 ± 0.04	0.78 ± 0.04	0.77 ± 0.04	0.77 ± 0.04	0.77 ± 0.04	0.78 ± 0.04	0.79 ± 0.04	0.80 ± 0.04
6.5	0.81 ± 0.04	0.81 ± 0.04	0.80 ± 0.04	0.80 ± 0.04	0.80 ± 0.04	0.80 ± 0.04	0.81 ± 0.04	0.82 ± 0.04
7.0	0.84 ± 0.04	0.83 ± 0.04	0.83 ± 0.04	0.82 ± 0.04	0.82 ± 0.04	0.82 ± 0.04	0.83 ± 0.04	0.84 ± 0.04
7.5	0.86 ± 0.04	0.86 ± 0.04	0.85 ± 0.04	0.85 ± 0.04	0.84 ± 0.04	0.84 ± 0.04	0.85 ± 0.04	0.85 ± 0.04
8.0	0.88 ± 0.04	0.88 ± 0.04	0.88 ± 0.04	0.87 ± 0.04	0.87 ± 0.04	0.87 ± 0.04	0.87 ± 0.04	0.87 ± 0.04
8.5	0.91 ± 0.04	0.91 ± 0.04	0.90 ± 0.04	0.89 ± 0.04	0.89 ± 0.04	0.89 ± 0.04	0.89 ± 0.04	0.89 ± 0.04
9.0	0.94 ± 0.04	0.93 ± 0.04	0.92 ± 0.04	0.91 ± 0.04	0.91 ± 0.04	0.91 ± 0.04	0.90 ± 0.04	0.91 ± 0.04
9.5	0.97 ± 0.04	0.96 ± 0.04	0.94 ± 0.04	0.94 ± 0.04	0.93 ± 0.04	0.92 ± 0.04	0.92 ± 0.04	0.92 ± 0.04
10.0	0.99 ± 0.05	0.98 ± 0.04	0.97 ± 0.04	0.96 ± 0.04	0.95 ± 0.04	0.94 ± 0.04	0.94 ± 0.04	0.94 ± 0.04

Table B.12. The contaminating fluxes (host galaxy + nearby companions) of ON 325 in mJy.

Aperture radius (arcsec)	*FWHM* (arcsec)						
	2.0	3.0	4.0	5.0	6.0	7.0	8.0
1.5	0.54 ± 0.09	0.59 ± 0.09	0.64 ± 0.09	0.69 ± 0.09	0.74 ± 0.09	0.78 ± 0.09	0.81 ± 0.09
2.0	0.59 ± 0.09	0.63 ± 0.09	0.67 ± 0.09	0.71 ± 0.09	0.75 ± 0.09	0.79 ± 0.09	0.82 ± 0.09
2.5	0.65 ± 0.09	0.67 ± 0.09	0.70 ± 0.09	0.74 ± 0.09	0.77 ± 0.09	0.80 ± 0.09	0.83 ± 0.09
3.0	0.70 ± 0.09	0.71 ± 0.09	0.73 ± 0.09	0.76 ± 0.09	0.79 ± 0.09	0.82 ± 0.09	0.85 ± 0.09
3.5	0.75 ± 0.09	0.75 ± 0.09	0.77 ± 0.09	0.79 ± 0.09	0.81 ± 0.09	0.84 ± 0.09	0.86 ± 0.09
4.0	0.8 ± 0.1	0.8 ± 0.1	0.80 ± 0.09	0.81 ± 0.09	0.83 ± 0.09	0.85 ± 0.09	0.87 ± 0.09
4.5	0.8 ± 0.1	0.8 ± 0.1	0.8 ± 0.1	0.84 ± 0.09	0.85 ± 0.09	0.87 ± 0.09	0.89 ± 0.09
5.0	0.9 ± 0.1	0.9 ± 0.1	0.9 ± 0.1	0.87 ± 0.09	0.88 ± 0.09	0.89 ± 0.09	0.91 ± 0.09
5.5	0.9 ± 0.1	0.9 ± 0.1	0.9 ± 0.1	0.89 ± 0.09	0.90 ± 0.09	0.91 ± 0.09	0.92 ± 0.09
6.0	0.9 ± 0.1	0.9 ± 0.1	0.9 ± 0.1	0.92 ± 0.09	0.92 ± 0.09	0.93 ± 0.09	0.94 ± 0.09
6.5	1.0 ± 0.1	0.9 ± 0.1	0.9 ± 0.1	0.94 ± 0.09	0.94 ± 0.09	0.95 ± 0.09	0.95 ± 0.09
7.0	1.0 ± 0.1	1.0 ± 0.1	0.96 ± 0.09	0.96 ± 0.09	0.96 ± 0.09	0.96 ± 0.09	0.97 ± 0.09
7.5	1.0 ± 0.1	1.0 ± 0.1	0.98 ± 0.09	0.98 ± 0.09	0.98 ± 0.09	0.98 ± 0.09	0.98 ± 0.09
8.0	1.0 ± 0.1	1.01 ± 0.09	1.00 ± 0.09	1.00 ± 0.09	1.00 ± 0.09	1.00 ± 0.09	1.00 ± 0.09
8.5	1.04 ± 0.09	1.03 ± 0.09	1.02 ± 0.09	1.02 ± 0.09	1.01 ± 0.09	1.01 ± 0.09	1.01 ± 0.09
9.0	1.05 ± 0.09	1.05 ± 0.09	1.04 ± 0.09	1.03 ± 0.09	1.03 ± 0.09	1.03 ± 0.09	1.03 ± 0.09
9.5	1.07 ± 0.09	1.06 ± 0.09	1.06 ± 0.09	1.05 ± 0.09	1.05 ± 0.09	1.04 ± 0.09	1.04 ± 0.09
10.0	1.09 ± 0.09	1.08 ± 0.09	1.07 ± 0.09	1.07 ± 0.09	1.06 ± 0.09	1.06 ± 0.09	1.06 ± 0.09

Table B.13. The contaminating fluxes (host galaxy + nearby companions) of 1ES 1218+304 in mJy.

Aperture radius (arcsec)	*FWHM* (arcsec)						
	2.0	3.0	4.0	5.0	6.0	7.0	8.0
2.0	0.21 ± 0.02	0.22 ± 0.02	0.25 ± 0.02	0.27 ± 0.02	0.29 ± 0.02	0.32 ± 0.02	0.34 ± 0.02
2.5	0.23 ± 0.02	0.24 ± 0.02	0.26 ± 0.02	0.28 ± 0.02	0.30 ± 0.02	0.33 ± 0.02	0.35 ± 0.02
3.0	0.26 ± 0.02	0.26 ± 0.02	0.28 ± 0.02	0.29 ± 0.02	0.31 ± 0.02	0.33 ± 0.02	0.36 ± 0.02
3.5	0.28 ± 0.02	0.28 ± 0.02	0.29 ± 0.02	0.31 ± 0.02	0.32 ± 0.02	0.34 ± 0.02	0.37 ± 0.02
4.0	0.30 ± 0.02	0.30 ± 0.02	0.31 ± 0.02	0.32 ± 0.02	0.34 ± 0.02	0.36 ± 0.02	0.38 ± 0.02
4.5	0.32 ± 0.02	0.32 ± 0.02	0.32 ± 0.02	0.33 ± 0.02	0.35 ± 0.02	0.37 ± 0.02	0.39 ± 0.02
5.0	0.34 ± 0.02	0.34 ± 0.02	0.34 ± 0.02	0.35 ± 0.02	0.36 ± 0.02	0.38 ± 0.02	0.40 ± 0.02
5.5	0.36 ± 0.02	0.35 ± 0.02	0.35 ± 0.02	0.36 ± 0.02	0.38 ± 0.02	0.39 ± 0.02	0.42 ± 0.02
6.0	0.37 ± 0.02	0.37 ± 0.02	0.37 ± 0.02	0.38 ± 0.02	0.39 ± 0.02	0.41 ± 0.02	0.43 ± 0.02
6.5	0.38 ± 0.02	0.38 ± 0.02	0.38 ± 0.02	0.39 ± 0.02	0.40 ± 0.02	0.42 ± 0.02	0.45 ± 0.02
7.0	0.39 ± 0.02	0.39 ± 0.02	0.40 ± 0.02	0.41 ± 0.02	0.42 ± 0.02	0.44 ± 0.02	0.47 ± 0.02
7.5	0.40 ± 0.02	0.40 ± 0.02	0.41 ± 0.02	0.42 ± 0.02	0.44 ± 0.02	0.46 ± 0.02	0.49 ± 0.02
8.0	0.41 ± 0.02	0.42 ± 0.02	0.42 ± 0.02	0.44 ± 0.02	0.45 ± 0.02	0.48 ± 0.02	0.51 ± 0.02
8.5	0.42 ± 0.02	0.43 ± 0.02	0.44 ± 0.02	0.45 ± 0.02	0.47 ± 0.02	0.50 ± 0.02	0.53 ± 0.02
9.0	0.43 ± 0.02	0.44 ± 0.02	0.45 ± 0.02	0.47 ± 0.02	0.49 ± 0.02	0.52 ± 0.02	0.56 ± 0.02
9.5	0.44 ± 0.02	0.45 ± 0.02	0.47 ± 0.02	0.49 ± 0.02	0.52 ± 0.02	0.55 ± 0.02	0.59 ± 0.02
10.0	0.45 ± 0.02	0.46 ± 0.02	0.49 ± 0.02	0.51 ± 0.02	0.55 ± 0.02	0.58 ± 0.02	0.62 ± 0.02

Table B.14. The contaminating fluxes (host galaxy + nearby companions) of RGB J1417+257 in mJy.

Aperture radius (arcsec)	*FWHM* (arcsec)							
	1.0	2.0	3.0	4.0	5.0	6.0	7.0	8.0
1.0	0.10 ± 0.03	0.14 ± 0.04	0.18 ± 0.04	0.21 ± 0.04	0.25 ± 0.04	0.29 ± 0.05	0.32 ± 0.05	0.35 ± 0.05
1.5	0.14 ± 0.04	0.16 ± 0.04	0.19 ± 0.04	0.23 ± 0.04	0.26 ± 0.05	0.29 ± 0.05	0.33 ± 0.05	0.36 ± 0.05
2.0	0.18 ± 0.04	0.19 ± 0.04	0.21 ± 0.04	0.24 ± 0.04	0.27 ± 0.05	0.31 ± 0.05	0.34 ± 0.05	0.36 ± 0.05
2.5	0.22 ± 0.04	0.22 ± 0.04	0.24 ± 0.04	0.26 ± 0.05	0.29 ± 0.05	0.32 ± 0.05	0.35 ± 0.05	0.37 ± 0.05
3.0	0.25 ± 0.05	0.25 ± 0.04	0.26 ± 0.05	0.28 ± 0.05	0.31 ± 0.05	0.33 ± 0.05	0.36 ± 0.05	0.38 ± 0.05
3.5	0.29 ± 0.05	0.28 ± 0.05	0.29 ± 0.05	0.31 ± 0.05	0.33 ± 0.05	0.35 ± 0.05	0.37 ± 0.05	0.39 ± 0.05
4.0	0.32 ± 0.05	0.32 ± 0.05	0.32 ± 0.05	0.33 ± 0.05	0.35 ± 0.05	0.37 ± 0.05	0.39 ± 0.05	0.40 ± 0.05
4.5	0.35 ± 0.05	0.35 ± 0.05	0.35 ± 0.05	0.36 ± 0.05	0.37 ± 0.05	0.39 ± 0.05	0.40 ± 0.05	0.42 ± 0.05
5.0	0.39 ± 0.05	0.39 ± 0.05	0.38 ± 0.05	0.39 ± 0.05	0.39 ± 0.05	0.40 ± 0.05	0.42 ± 0.05	0.43 ± 0.05
5.5	0.43 ± 0.05	0.42 ± 0.05	0.41 ± 0.05	0.41 ± 0.05	0.42 ± 0.05	0.42 ± 0.05	0.43 ± 0.05	0.45 ± 0.05
6.0	0.47 ± 0.05	0.45 ± 0.05	0.44 ± 0.05	0.44 ± 0.05	0.44 ± 0.05	0.44 ± 0.05	0.45 ± 0.05	0.46 ± 0.05
6.5	0.50 ± 0.05	0.48 ± 0.05	0.47 ± 0.05	0.46 ± 0.05	0.46 ± 0.05	0.46 ± 0.05	0.47 ± 0.05	0.47 ± 0.05
7.0	0.52 ± 0.06	0.51 ± 0.06	0.49 ± 0.06	0.49 ± 0.05	0.48 ± 0.05	0.48 ± 0.05	0.48 ± 0.06	0.49 ± 0.06
7.5	0.54 ± 0.06	0.53 ± 0.06	0.52 ± 0.06	0.51 ± 0.06	0.50 ± 0.06	0.50 ± 0.06	0.50 ± 0.06	0.50 ± 0.06
8.0	0.56 ± 0.06	0.55 ± 0.06	0.54 ± 0.06	0.53 ± 0.06	0.52 ± 0.06	0.52 ± 0.06	0.51 ± 0.06	0.51 ± 0.06
8.5	0.57 ± 0.06	0.56 ± 0.06	0.55 ± 0.06	0.54 ± 0.06	0.54 ± 0.06	0.53 ± 0.06	0.53 ± 0.06	0.53 ± 0.06
9.0	0.59 ± 0.06	0.58 ± 0.06	0.57 ± 0.06	0.56 ± 0.06	0.55 ± 0.06	0.54 ± 0.06	0.54 ± 0.06	0.54 ± 0.06
9.5	0.60 ± 0.06	0.59 ± 0.06	0.58 ± 0.06	0.57 ± 0.06	0.56 ± 0.06	0.56 ± 0.06	0.55 ± 0.06	0.55 ± 0.06
10.0	0.61 ± 0.06	0.60 ± 0.06	0.59 ± 0.06	0.59 ± 0.06	0.58 ± 0.06	0.57 ± 0.06	0.56 ± 0.06	0.56 ± 0.06

Table B.15. The contaminating fluxes (host galaxy + nearby companions) of 1ES 1426+428 in mJy.

Aperture radius (arcsec)	*FWHM* (arcsec)							
	1.0	2.0	3.0	4.0	5.0	6.0	7.0	8.0
1.0	0.29 ± 0.02	0.36 ± 0.02	0.43 ± 0.02	0.50 ± 0.02	0.56 ± 0.02	0.61 ± 0.02	0.65 ± 0.03	0.69 ± 0.03
1.5	0.38 ± 0.02	0.41 ± 0.02	0.47 ± 0.02	0.52 ± 0.02	0.57 ± 0.02	0.62 ± 0.03	0.66 ± 0.03	0.70 ± 0.03
2.0	0.46 ± 0.02	0.47 ± 0.02	0.51 ± 0.02	0.55 ± 0.02	0.59 ± 0.02	0.64 ± 0.03	0.67 ± 0.03	0.71 ± 0.03
2.5	0.53 ± 0.02	0.53 ± 0.02	0.55 ± 0.02	0.58 ± 0.02	0.62 ± 0.03	0.65 ± 0.03	0.69 ± 0.03	0.72 ± 0.03
3.0	0.59 ± 0.02	0.58 ± 0.02	0.59 ± 0.02	0.61 ± 0.02	0.64 ± 0.03	0.67 ± 0.03	0.70 ± 0.03	0.73 ± 0.03
3.5	0.65 ± 0.03	0.63 ± 0.03	0.63 ± 0.03	0.65 ± 0.03	0.67 ± 0.03	0.69 ± 0.03	0.72 ± 0.03	0.75 ± 0.03
4.0	0.69 ± 0.03	0.68 ± 0.03	0.67 ± 0.03	0.68 ± 0.03	0.70 ± 0.03	0.72 ± 0.03	0.74 ± 0.03	0.76 ± 0.03
4.5	0.74 ± 0.03	0.72 ± 0.03	0.71 ± 0.03	0.71 ± 0.03	0.72 ± 0.03	0.74 ± 0.03	0.76 ± 0.03	0.78 ± 0.03
5.0	0.77 ± 0.03	0.76 ± 0.03	0.75 ± 0.03	0.75 ± 0.03	0.75 ± 0.03	0.76 ± 0.03	0.78 ± 0.03	0.79 ± 0.03
5.5	0.80 ± 0.03	0.79 ± 0.03	0.78 ± 0.03	0.78 ± 0.03	0.78 ± 0.03	0.79 ± 0.03	0.80 ± 0.03	0.81 ± 0.03
6.0	0.83 ± 0.03	0.82 ± 0.03	0.81 ± 0.03	0.80 ± 0.03	0.80 ± 0.03	0.81 ± 0.03	0.82 ± 0.03	0.83 ± 0.03
6.5	0.86 ± 0.03	0.85 ± 0.03	0.84 ± 0.03	0.83 ± 0.03	0.83 ± 0.03	0.83 ± 0.03	0.84 ± 0.03	0.84 ± 0.03
7.0	0.88 ± 0.04	0.87 ± 0.03	0.86 ± 0.03	0.85 ± 0.03	0.85 ± 0.03	0.85 ± 0.03	0.85 ± 0.03	0.86 ± 0.03
7.5	0.91 ± 0.04	0.90 ± 0.04	0.89 ± 0.03	0.88 ± 0.03	0.87 ± 0.03	0.87 ± 0.03	0.87 ± 0.03	0.88 ± 0.03
8.0	0.93 ± 0.04	0.92 ± 0.04	0.91 ± 0.04	0.90 ± 0.04	0.89 ± 0.03	0.89 ± 0.03	0.89 ± 0.03	0.89 ± 0.03
8.5	0.94 ± 0.04	0.94 ± 0.04	0.93 ± 0.04	0.92 ± 0.04	0.91 ± 0.04	0.91 ± 0.04	0.91 ± 0.04	0.91 ± 0.04
9.0	0.96 ± 0.04	0.95 ± 0.04	0.95 ± 0.04	0.94 ± 0.04	0.93 ± 0.04	0.93 ± 0.04	0.92 ± 0.04	0.93 ± 0.04
9.5	0.98 ± 0.04	0.97 ± 0.04	0.96 ± 0.04	0.95 ± 0.04	0.95 ± 0.04	0.94 ± 0.04	0.94 ± 0.04	0.94 ± 0.04
10.0	0.99 ± 0.04	0.99 ± 0.04	0.98 ± 0.04	0.97 ± 0.04	0.96 ± 0.04	0.96 ± 0.04	0.96 ± 0.04	0.95 ± 0.04

Table B.16. The contaminating fluxes (host galaxy + nearby companions) of 1ES 1544+820 in mJy.

Aperture radius (arcsec)	*FWHM* (arcsec)						
	2.0	3.0	4.0	5.0	6.0	7.0	8.0
2.0	0.01 ± 0.01	0.02 ± 0.01	0.04 ± 0.01	0.06 ± 0.01	0.08 ± 0.01	0.10 ± 0.01	0.12 ± 0.01
2.5	0.02 ± 0.01	0.03 ± 0.01	0.05 ± 0.01	0.07 ± 0.01	0.09 ± 0.01	0.11 ± 0.01	0.12 ± 0.01
3.0	0.03 ± 0.01	0.05 ± 0.01	0.07 ± 0.01	0.08 ± 0.01	0.10 ± 0.01	0.11 ± 0.01	0.13 ± 0.01
3.5	0.06 ± 0.01	0.07 ± 0.01	0.09 ± 0.01	0.10 ± 0.01	0.11 ± 0.01	0.12 ± 0.01	0.13 ± 0.01
4.0	0.09 ± 0.01	0.10 ± 0.01	0.10 ± 0.01	0.11 ± 0.01	0.12 ± 0.01	0.13 ± 0.01	0.14 ± 0.01
4.5	0.13 ± 0.01	0.12 ± 0.01	0.12 ± 0.01	0.13 ± 0.01	0.13 ± 0.01	0.14 ± 0.01	0.15 ± 0.01
5.0	0.17 ± 0.01	0.15 ± 0.01	0.14 ± 0.01	0.14 ± 0.01	0.15 ± 0.01	0.15 ± 0.01	0.15 ± 0.01
5.5	0.19 ± 0.01	0.17 ± 0.01	0.16 ± 0.01	0.16 ± 0.01	0.16 ± 0.01	0.16 ± 0.01	0.16 ± 0.01
6.0	0.20 ± 0.01	0.18 ± 0.01	0.17 ± 0.01	0.17 ± 0.01	0.17 ± 0.01	0.17 ± 0.01	0.17 ± 0.01
6.5	0.21 ± 0.01	0.20 ± 0.01	0.19 ± 0.01	0.18 ± 0.01	0.18 ± 0.01	0.17 ± 0.01	0.17 ± 0.01
7.0	0.21 ± 0.01	0.20 ± 0.01	0.19 ± 0.01	0.19 ± 0.01	0.18 ± 0.01	0.18 ± 0.01	0.18 ± 0.01
7.5	0.21 ± 0.01	0.21 ± 0.01	0.20 ± 0.01	0.19 ± 0.01	0.19 ± 0.01	0.19 ± 0.01	0.19 ± 0.01
8.0	0.22 ± 0.01	0.21 ± 0.01	0.20 ± 0.01	0.20 ± 0.01	0.19 ± 0.01	0.19 ± 0.01	0.19 ± 0.01
8.5	0.22 ± 0.01	0.21 ± 0.01	0.21 ± 0.01	0.20 ± 0.01	0.20 ± 0.01	0.20 ± 0.01	0.19 ± 0.01
9.0	0.22 ± 0.01	0.21 ± 0.01	0.21 ± 0.01	0.21 ± 0.01	0.20 ± 0.01	0.20 ± 0.01	0.20 ± 0.01
9.5	0.22 ± 0.01	0.22 ± 0.01	0.21 ± 0.01	0.21 ± 0.01	0.21 ± 0.01	0.20 ± 0.01	0.20 ± 0.01
10.0	0.22 ± 0.01	0.22 ± 0.01	0.21 ± 0.01	0.21 ± 0.01	0.21 ± 0.01	0.21 ± 0.01	0.20 ± 0.01

Table B.17. The contaminating fluxes (host galaxy + nearby companions) of Mrk 501 in mJy.

Aperture radius (arcsec)	*FWHM* (arcsec)							
	1.0	2.0	3.0	4.0	5.0	6.0	7.0	8.0
1.0	3.4 ± 0.2	4.1 ± 0.2	5.1 ± 0.2	6.0 ± 0.2	6.8 ± 0.2	7.5 ± 0.2	8.2 ± 0.2	8.9 ± 0.2
1.5	4.4 ± 0.2	4.8 ± 0.2	5.5 ± 0.2	6.3 ± 0.2	7.0 ± 0.2	7.7 ± 0.2	8.4 ± 0.2	9.0 ± 0.2
2.0	5.3 ± 0.2	5.5 ± 0.2	6.0 ± 0.2	6.6 ± 0.2	7.3 ± 0.2	7.9 ± 0.2	8.6 ± 0.2	9.2 ± 0.2
2.5	6.2 ± 0.2	6.2 ± 0.2	6.6 ± 0.2	7.1 ± 0.2	7.6 ± 0.2	8.2 ± 0.2	8.8 ± 0.2	9.3 ± 0.2
3.0	7.1 ± 0.2	7.0 ± 0.2	7.2 ± 0.2	7.5 ± 0.2	8.0 ± 0.2	8.5 ± 0.2	9.0 ± 0.2	9.5 ± 0.2
3.5	7.8 ± 0.2	7.7 ± 0.2	7.8 ± 0.2	8.0 ± 0.2	8.4 ± 0.2	8.8 ± 0.2	9.3 ± 0.2	9.8 ± 0.2
4.0	8.5 ± 0.2	8.4 ± 0.2	8.4 ± 0.2	8.5 ± 0.2	8.8 ± 0.2	9.2 ± 0.2	9.6 ± 0.2	10.0 ± 0.3
4.5	9.2 ± 0.2	9.0 ± 0.2	8.9 ± 0.2	9.1 ± 0.2	9.3 ± 0.2	9.6 ± 0.2	9.9 ± 0.3	10.3 ± 0.3
5.0	9.8 ± 0.3	9.6 ± 0.2	9.5 ± 0.2	9.6 ± 0.2	9.7 ± 0.2	10.0 ± 0.3	10.3 ± 0.3	10.6 ± 0.3
5.5	10.3 ± 0.3	10.2 ± 0.3	10.1 ± 0.3	10.1 ± 0.3	10.2 ± 0.3	10.4 ± 0.3	10.6 ± 0.3	10.9 ± 0.3
6.0	10.9 ± 0.3	10.7 ± 0.3	10.6 ± 0.3	10.6 ± 0.3	10.6 ± 0.3	10.8 ± 0.3	11.0 ± 0.3	11.2 ± 0.3
6.5	11.4 ± 0.3	11.2 ± 0.3	11.1 ± 0.3	11.0 ± 0.3	11.1 ± 0.3	11.2 ± 0.3	11.3 ± 0.3	11.6 ± 0.3
7.0	11.8 ± 0.3	11.7 ± 0.3	11.6 ± 0.3	11.5 ± 0.3	11.5 ± 0.3	11.6 ± 0.3	11.7 ± 0.3	11.9 ± 0.3
7.5	12.3 ± 0.3	12.2 ± 0.3	12.0 ± 0.3	12.0 ± 0.3	11.9 ± 0.3	12.0 ± 0.3	12.1 ± 0.3	12.2 ± 0.3
8.0	12.7 ± 0.3	12.6 ± 0.3	12.5 ± 0.3	12.4 ± 0.3	12.3 ± 0.3	12.4 ± 0.3	12.4 ± 0.3	12.6 ± 0.3
8.5	13.2 ± 0.3	13.0 ± 0.3	12.9 ± 0.3	12.8 ± 0.3	12.8 ± 0.3	12.7 ± 0.3	12.8 ± 0.3	12.9 ± 0.3
9.0	13.6 ± 0.3	13.5 ± 0.3	13.3 ± 0.3	13.2 ± 0.3	13.1 ± 0.3	13.1 ± 0.3	13.2 ± 0.3	13.2 ± 0.3
9.5	14.0 ± 0.3	13.8 ± 0.3	13.7 ± 0.3	13.6 ± 0.3	13.5 ± 0.3	13.5 ± 0.3	13.5 ± 0.3	13.6 ± 0.3
10.0	14.3 ± 0.4	14.2 ± 0.3	14.1 ± 0.3	14.0 ± 0.3	13.9 ± 0.3	13.9 ± 0.3	13.8 ± 0.3	13.9 ± 0.3

Table B.18. The contaminating fluxes (host galaxy + nearby companions) of OT 546 in mJy.

Aperture radius (arcsec)	*FWHM* (arcsec)					
	3.0	4.0	5.0	6.0	7.0	8.0
2.5	0.70 ± 0.05	0.75 ± 0.05	0.81 ± 0.05	0.87 ± 0.05	0.93 ± 0.05	0.98 ± 0.05
3.0	0.77 ± 0.05	0.80 ± 0.05	0.85 ± 0.05	0.90 ± 0.05	0.95 ± 0.05	1.00 ± 0.05
3.5	0.83 ± 0.05	0.86 ± 0.05	0.89 ± 0.05	0.93 ± 0.05	0.98 ± 0.05	1.02 ± 0.05
4.0	0.90 ± 0.06	0.91 ± 0.05	0.94 ± 0.05	0.97 ± 0.05	1.01 ± 0.05	1.04 ± 0.05
4.5	0.96 ± 0.06	0.96 ± 0.06	0.98 ± 0.05	1.01 ± 0.05	1.04 ± 0.05	1.07 ± 0.05
5.0	1.01 ± 0.06	1.01 ± 0.06	1.02 ± 0.06	1.04 ± 0.05	1.07 ± 0.05	1.10 ± 0.05
5.5	1.07 ± 0.06	1.06 ± 0.06	1.07 ± 0.06	1.08 ± 0.06	1.10 ± 0.05	1.13 ± 0.05
6.0	1.12 ± 0.06	1.11 ± 0.06	1.11 ± 0.06	1.12 ± 0.06	1.13 ± 0.05	1.15 ± 0.06
6.5	1.16 ± 0.06	1.15 ± 0.06	1.15 ± 0.06	1.16 ± 0.06	1.17 ± 0.06	1.18 ± 0.06
7.0	1.21 ± 0.06	1.19 ± 0.06	1.19 ± 0.06	1.19 ± 0.06	1.20 ± 0.06	1.21 ± 0.06
7.5	1.25 ± 0.06	1.23 ± 0.06	1.23 ± 0.06	1.23 ± 0.06	1.23 ± 0.06	1.24 ± 0.06
8.0	1.28 ± 0.06	1.27 ± 0.06	1.26 ± 0.06	1.26 ± 0.06	1.26 ± 0.06	1.27 ± 0.06
8.5	1.32 ± 0.06	1.30 ± 0.06	1.29 ± 0.06	1.29 ± 0.06	1.29 ± 0.06	1.29 ± 0.06
9.0	1.35 ± 0.06	1.34 ± 0.06	1.33 ± 0.06	1.32 ± 0.06	1.32 ± 0.06	1.32 ± 0.06
9.5	1.38 ± 0.06	1.37 ± 0.06	1.36 ± 0.06	1.35 ± 0.06	1.34 ± 0.06	1.34 ± 0.06
10.0	1.41 ± 0.06	1.39 ± 0.06	1.38 ± 0.06	1.38 ± 0.06	1.37 ± 0.06	1.37 ± 0.06

Table B.19. The contaminating fluxes (host galaxy + nearby companions) of 1ES 1959+650 in mJy.

Aperture radius (arcsec)	*FWHM* (arcsec)							
	1.0	2.0	3.0	4.0	5.0	6.0	7.0	8.0
1.0	0.25 ± 0.01	0.37 ± 0.01	0.51 ± 0.02	0.65 ± 0.02	0.79 ± 0.02	0.92 ± 0.02	1.04 ± 0.03	1.16 ± 0.03
1.5	0.38 ± 0.02	0.46 ± 0.02	0.57 ± 0.02	0.70 ± 0.02	0.83 ± 0.02	0.95 ± 0.02	1.07 ± 0.03	1.18 ± 0.03
2.0	0.53 ± 0.02	0.56 ± 0.02	0.65 ± 0.02	0.76 ± 0.02	0.87 ± 0.02	0.99 ± 0.03	1.10 ± 0.03	1.20 ± 0.03
2.5	0.67 ± 0.02	0.68 ± 0.02	0.74 ± 0.02	0.83 ± 0.02	0.93 ± 0.02	1.03 ± 0.03	1.14 ± 0.03	1.24 ± 0.03
3.0	0.81 ± 0.02	0.80 ± 0.02	0.84 ± 0.02	0.91 ± 0.02	0.99 ± 0.03	1.08 ± 0.03	1.18 ± 0.03	1.27 ± 0.03
3.5	0.94 ± 0.02	0.93 ± 0.02	0.94 ± 0.02	0.99 ± 0.03	1.06 ± 0.03	1.14 ± 0.03	1.23 ± 0.03	1.32 ± 0.03
4.0	1.07 ± 0.03	1.04 ± 0.03	1.05 ± 0.03	1.08 ± 0.03	1.14 ± 0.03	1.21 ± 0.03	1.28 ± 0.03	1.36 ± 0.03
4.5	1.18 ± 0.03	1.16 ± 0.03	1.15 ± 0.03	1.17 ± 0.03	1.22 ± 0.03	1.27 ± 0.03	1.34 ± 0.03	1.41 ± 0.03
5.0	1.29 ± 0.03	1.26 ± 0.03	1.25 ± 0.03	1.26 ± 0.03	1.30 ± 0.03	1.34 ± 0.03	1.40 ± 0.03	1.47 ± 0.04
5.5	1.39 ± 0.03	1.36 ± 0.03	1.35 ± 0.03	1.35 ± 0.03	1.38 ± 0.03	1.42 ± 0.03	1.47 ± 0.03	1.53 ± 0.04
6.0	1.49 ± 0.03	1.46 ± 0.03	1.44 ± 0.03	1.44 ± 0.03	1.46 ± 0.03	1.49 ± 0.03	1.54 ± 0.04	1.59 ± 0.04
6.5	1.57 ± 0.04	1.55 ± 0.03	1.53 ± 0.03	1.53 ± 0.04	1.54 ± 0.04	1.57 ± 0.04	1.60 ± 0.04	1.65 ± 0.04
7.0	1.65 ± 0.04	1.63 ± 0.04	1.61 ± 0.04	1.61 ± 0.04	1.62 ± 0.04	1.64 ± 0.04	1.67 ± 0.04	1.71 ± 0.04
7.5	1.73 ± 0.04	1.71 ± 0.04	1.70 ± 0.04	1.70 ± 0.04	1.70 ± 0.04	1.72 ± 0.04	1.75 ± 0.04	1.78 ± 0.04
8.0	1.80 ± 0.04	1.79 ± 0.04	1.78 ± 0.04	1.78 ± 0.04	1.79 ± 0.04	1.80 ± 0.04	1.82 ± 0.04	1.85 ± 0.05
8.5	1.87 ± 0.04	1.87 ± 0.04	1.87 ± 0.04	1.87 ± 0.04	1.87 ± 0.04	1.88 ± 0.04	1.89 ± 0.05	1.91 ± 0.05
9.0	1.93 ± 0.05	1.95 ± 0.05	1.96 ± 0.05	1.96 ± 0.05	1.96 ± 0.05	1.96 ± 0.05	1.97 ± 0.05	1.98 ± 0.05
9.5	2.01 ± 0.05	2.05 ± 0.05	2.06 ± 0.05	2.05 ± 0.05	2.05 ± 0.05	2.04 ± 0.05	2.04 ± 0.05	2.05 ± 0.05
10.0	2.14 ± 0.05	2.17 ± 0.05	2.17 ± 0.05	2.15 ± 0.05	2.13 ± 0.05	2.12 ± 0.05	2.11 ± 0.05	2.11 ± 0.06

Table B.20. The contaminating fluxes (host galaxy + nearby companions) of BL Lac in mJy.

Aperture radius (arcsec)	*FWHM* (arcsec)							
	1.0	2.0	3.0	4.0	5.0	6.0	7.0	8.0
1.0	0.35 ± 0.02	0.45 ± 0.02	0.56 ± 0.02	0.67 ± 0.02	0.77 ± 0.03	0.86 ± 0.03	0.94 ± 0.04	1.01 ± 0.06
1.5	0.47 ± 0.02	0.53 ± 0.02	0.61 ± 0.02	0.71 ± 0.02	0.80 ± 0.03	0.88 ± 0.03	0.96 ± 0.04	1.03 ± 0.06
2.0	0.60 ± 0.02	0.62 ± 0.02	0.68 ± 0.02	0.75 ± 0.03	0.83 ± 0.03	0.91 ± 0.03	0.98 ± 0.04	1.05 ± 0.06
2.5	0.71 ± 0.03	0.71 ± 0.03	0.74 ± 0.03	0.80 ± 0.03	0.87 ± 0.03	0.94 ± 0.03	1.00 ± 0.04	1.07 ± 0.06
3.0	0.81 ± 0.03	0.80 ± 0.03	0.82 ± 0.03	0.86 ± 0.03	0.91 ± 0.03	0.97 ± 0.03	1.03 ± 0.05	1.09 ± 0.06
3.5	0.90 ± 0.03	0.88 ± 0.03	0.89 ± 0.03	0.92 ± 0.03	0.96 ± 0.03	1.01 ± 0.04	1.07 ± 0.05	1.12 ± 0.07
4.0	0.98 ± 0.03	0.96 ± 0.03	0.96 ± 0.03	0.98 ± 0.03	1.01 ± 0.03	1.06 ± 0.04	1.10 ± 0.05	1.15 ± 0.07
4.5	1.06 ± 0.03	1.04 ± 0.03	1.03 ± 0.03	1.04 ± 0.03	1.07 ± 0.03	1.10 ± 0.04	1.14 ± 0.05	1.18 ± 0.08
5.0	1.13 ± 0.03	1.11 ± 0.03	1.10 ± 0.03	1.10 ± 0.03	1.12 ± 0.03	1.14 ± 0.04	1.18 ± 0.06	1.21 ± 0.08
5.5	1.20 ± 0.03	1.18 ± 0.03	1.16 ± 0.03	1.16 ± 0.03	1.17 ± 0.04	1.19 ± 0.05	1.22 ± 0.06	1.25 ± 0.09
6.0	1.26 ± 0.03	1.24 ± 0.03	1.22 ± 0.03	1.22 ± 0.03	1.22 ± 0.04	1.24 ± 0.05	1.26 ± 0.07	1.3 ± 0.1
6.5	1.32 ± 0.03	1.30 ± 0.03	1.28 ± 0.03	1.27 ± 0.03	1.27 ± 0.04	1.28 ± 0.06	1.30 ± 0.08	1.3 ± 0.1
7.0	1.37 ± 0.03	1.35 ± 0.03	1.33 ± 0.03	1.32 ± 0.04	1.32 ± 0.05	1.32 ± 0.06	1.34 ± 0.09	1.4 ± 0.2
7.5	1.42 ± 0.03	1.40 ± 0.03	1.38 ± 0.03	1.37 ± 0.04	1.37 ± 0.05	1.37 ± 0.07	1.38 ± 0.09	1.4 ± 0.2
8.0	1.47 ± 0.03	1.45 ± 0.03	1.43 ± 0.04	1.42 ± 0.04	1.41 ± 0.06	1.41 ± 0.08	1.4 ± 0.1	1.4 ± 0.2
8.5	1.51 ± 0.03	1.50 ± 0.03	1.48 ± 0.04	1.46 ± 0.05	1.45 ± 0.07	1.45 ± 0.09	1.5 ± 0.2	1.5 ± 0.2
9.0	1.55 ± 0.04	1.54 ± 0.04	1.52 ± 0.05	1.51 ± 0.06	1.50 ± 0.07	1.5 ± 0.1	1.5 ± 0.2	1.5 ± 0.2
9.5	1.59 ± 0.04	1.58 ± 0.04	1.56 ± 0.05	1.55 ± 0.07	1.54 ± 0.08	1.5 ± 0.2	1.5 ± 0.2	1.5 ± 0.2
10.0	1.63 ± 0.04	1.62 ± 0.05	1.60 ± 0.06	1.59 ± 0.07	1.6 ± 0.1	1.6 ± 0.2	1.6 ± 0.2	1.6 ± 0.2

Table B.21. The contaminating fluxes (host galaxy + nearby companions) of 1ES 2344+514 in mJy.

Aperture radius (arcsec)	*FWHM* (arcsec)							
	1.0	2.0	3.0	4.0	5.0	6.0	7.0	8.0
1.0	0.88 ± 0.03	1.13 ± 0.03	1.44 ± 0.03	1.73 ± 0.03	2.00 ± 0.03	2.25 ± 0.04	2.49 ± 0.04	2.72 ± 0.04
1.5	1.20 ± 0.03	1.34 ± 0.03	1.57 ± 0.03	1.83 ± 0.03	2.07 ± 0.03	2.31 ± 0.04	2.54 ± 0.04	2.76 ± 0.04
2.0	1.52 ± 0.03	1.57 ± 0.03	1.74 ± 0.03	1.95 ± 0.03	2.17 ± 0.04	2.39 ± 0.04	2.60 ± 0.04	2.82 ± 0.04
2.5	1.81 ± 0.03	1.82 ± 0.03	1.93 ± 0.03	2.09 ± 0.04	2.28 ± 0.04	2.48 ± 0.04	2.68 ± 0.04	2.88 ± 0.04
3.0	2.09 ± 0.04	2.06 ± 0.04	2.12 ± 0.04	2.24 ± 0.04	2.40 ± 0.04	2.58 ± 0.04	2.76 ± 0.04	2.95 ± 0.04
3.5	2.34 ± 0.04	2.29 ± 0.04	2.32 ± 0.04	2.41 ± 0.04	2.54 ± 0.04	2.69 ± 0.04	2.86 ± 0.04	3.03 ± 0.04
4.0	2.57 ± 0.04	2.52 ± 0.04	2.52 ± 0.04	2.58 ± 0.04	2.68 ± 0.04	2.81 ± 0.04	2.96 ± 0.04	3.12 ± 0.04
4.5	2.78 ± 0.04	2.73 ± 0.04	2.71 ± 0.04	2.75 ± 0.04	2.83 ± 0.04	2.94 ± 0.04	3.07 ± 0.04	3.22 ± 0.04
5.0	2.98 ± 0.04	2.92 ± 0.04	2.90 ± 0.04	2.91 ± 0.04	2.98 ± 0.04	3.07 ± 0.04	3.19 ± 0.04	3.32 ± 0.04
5.5	3.16 ± 0.04	3.11 ± 0.04	3.07 ± 0.04	3.08 ± 0.04	3.13 ± 0.04	3.21 ± 0.04	3.31 ± 0.04	3.44 ± 0.05
6.0	3.33 ± 0.05	3.28 ± 0.04	3.25 ± 0.04	3.24 ± 0.04	3.28 ± 0.04	3.34 ± 0.04	3.44 ± 0.04	3.55 ± 0.05
6.5	3.49 ± 0.05	3.45 ± 0.05	3.41 ± 0.04	3.40 ± 0.04	3.43 ± 0.04	3.48 ± 0.04	3.57 ± 0.05	3.67 ± 0.05
7.0	3.65 ± 0.05	3.60 ± 0.05	3.56 ± 0.05	3.55 ± 0.05	3.57 ± 0.05	3.62 ± 0.05	3.70 ± 0.05	3.80 ± 0.05
7.5	3.79 ± 0.05	3.75 ± 0.05	3.71 ± 0.05	3.70 ± 0.05	3.72 ± 0.05	3.77 ± 0.05	3.84 ± 0.05	3.93 ± 0.05
8.0	3.92 ± 0.05	3.89 ± 0.05	3.86 ± 0.05	3.85 ± 0.05	3.87 ± 0.05	3.91 ± 0.05	3.98 ± 0.05	4.07 ± 0.05
8.5	4.05 ± 0.05	4.02 ± 0.05	4.00 ± 0.05	3.99 ± 0.05	4.01 ± 0.05	4.06 ± 0.05	4.12 ± 0.05	4.20 ± 0.05
9.0	4.17 ± 0.05	4.15 ± 0.05	4.13 ± 0.05	4.14 ± 0.05	4.16 ± 0.05	4.21 ± 0.05	4.27 ± 0.05	4.35 ± 0.05
9.5	4.28 ± 0.05	4.27 ± 0.05	4.27 ± 0.05	4.28 ± 0.05	4.32 ± 0.05	4.37 ± 0.05	4.43 ± 0.05	4.50 ± 0.05
10.0	4.40 ± 0.05	4.39 ± 0.05	4.40 ± 0.05	4.44 ± 0.05	4.48 ± 0.05	4.53 ± 0.05	4.59 ± 0.05	4.66 ± 0.06